Deep Controlled Source Electro-Magnetic Sensing: A Cost Effective, Long-Term Tool for Sequestration Monitoring

Final Technical Report

Reporting/Project Period: October 1, 2013 – December 31, 2016

Report Number: DOE-MPT-0012266

Principal Authors:

Dr. Douglas LaBrecque and Russell Brigham

Additional Authors:

Conny Schmidt-Hattenburger, Even Um, Peter Petrov and Thomas Daley

Product Date: January 31, 2017

Project Number: DE-FE0012266

for

U.S. Department of Energy

National Energy Technology Laboratory

Performing Organization:

Multi-Phase Technologies, LLC

1430 Greg Street, Ste. 503

Sparks, NV 89431

Other Team Members:

Lawrence Berkeley National Laboratory and GFZ German Research Centre for Geoscience

Principal Investigator: Dr. Douglas LaBrecque

dlabrecque@mpt3d.com

Submitting Official: Russell Brigham

rbrigham@mpt3d.com

Disclaimer

Table of Contents

List of Acronyms and Abbreviations

3D	Three Dimension
By	Magnetic Response
CO_2	Carbon Dioxide
CSEM	Controlled-source electromagnetic
DC	Direct Current
DOE	Department of Energy
EM	Electromagnetic
ERT	Electrical Resistivity Tomography
Ex	Voltage Response
FD	Finite-Difference
FDIP	Frequency Domain IP
GFZ	Helmholtz Centre Potsdam German Research Centre for Geosciences
Hz	Hertz
LBNL	Lawrence Berkeley National Laboratory
m	Meters
MMR	Magnetometric Resistivity
MSR	Multi-Source units
MVA	Monitoring, Verification and Accounting
NERSC	National Energy Research Scientific Computing Center
NETL	National Energy Technology Laboratory
Ohm-m	Ohm meters
PLPT	Pyramid Lake Paiute Tribe, Nevada
TDIP	Time-Domain IP
STB	Surface to Borehole
V	Volts
XERT	Cross Electrical Resistivity Tomography (Cross Borehole ERT)
Z	Vertical

Acknowledgements

This work was completed as part of National Energy Technology Laboratory (NETL) research for the U.S. Department of Energy's (DOE) Advanced Technologies for Monitoring Carbon Dioxide (CO_2) in Geologic Storage and Utilization Operations. The authors wish to acknowledge Karen Kluger and Jerry Carr (NETL Federal Project Managers) for guidance, direction, and support, Tim Labitzke for his assistance in carrying out field operations, Mr. Schuster for coordinating permitted entry schedules with the local farmers, and the support from the Helmholtz Centre Potsdam German Research Centre for Geosciences and the Pyramid Lake Paiute Tribe for allowing access to the Astor Pass Geothermal site.

Executive Summary

The goal of the Carbon Storage Program is to develop and validate technologies to enhance the monitoring, verification, and accounting (MVA) of CO_2 injected underground. This MVA will be applied to long-term storage of CO_2 and may also be a method to enhance recovery of oil and gas reserves. Assessing inventories of CO_2 and assuring that those inventories stay within the bounds of the reservoir, as well as monitoring for recovery of fossil fuels, are extremely difficult problems. Using dense arrays of wells for monitoring CO_2 inventories is not practical. First, the cost of such wells is prohibitively high and second, installing a large number of monitoring wells substantially increases the risk of leakage. Because of this, most existing or planned sequestration sites have (or will have) few monitoring wells. Because of the natural variability of storage reservoirs, it is impossible to arrive at a reliable appraisal of CO_2 inventories with only one or two measurement points.

High resolution, three-dimensional (3D) seismic surveys are very good at providing structure information on reservoirs and can provide estimates of supercritical/gas phase CO_2 at reservoir depths with sufficient horizontal and vertical accuracy (Arts et al., 2004; White, 2009; Ivanova et al., 2012). However, a major limitation of the 3D seismic method is cost; at present, a large scale 3D seismic survey generally costs millions of dollars. This limits the use of 3D seismic surveys to relatively infrequent - likely five or ten year - intervals. A second limitation of the seismic method is that it is insensitive to dissolved phase CO_2 both in the reservoir and in shallower locations such as drinking water sources.

An alternative and complementary geophysical method is controlled source electromagnetic measurements (CSEM). Deep CSEM uses low-frequency (generally ranging from a fraction of a Hertz to a few Hertz) to provide estimates of formation electrical properties down to oil field depths (see for example Constable, 2010). The source is generally a pair of widely separated electrodes used to inject current into the formation (referred to as a dipole) and a combination of electric and magnetic field receivers some distance away from the source. Deep CSEM has the potential to provide the basis for a cost-effective strategy to monitor storage or movement of supercritical and gas phase CO_2 and changes in dissolved phase CO_2 within underground reservoirs (Gasperikova and Hoversten, 2006).

When supercritical CO_2 is injected into an aquifer, the resistive CO_2 displaces the electrically conductive pore fluids, which results in an increase of resistivity (Gasperikova and Hoversten, 2006, Kiessling et al., 2010, Yang et al., 2012). The relationship between electrical resistivity and saturation is well known, particularly in the type of highly saline aquifers present in a typical oil field and the types of deep aquifers suitable for long-term CO_2 storage.

Away from the primary reservoir, any long-term leakage of dissolved phase CO_2 is expected to produce the opposite, but equally strong, effect of decreasing electrical resistivity by increasing the ionic content of the pore water. This process is a current research topic and likely involves both the direct solution of CO_2 and solution of ions and minerals from the surrounding formation due to decreased pH when the CO_2 forms carbonic acid.

If enough spatial resolution is achieved, electrical resistivity measurements have the potential to provide a method of monitoring the primary inventory of CO_2 as well as track the migration and estimate the volume of CO_2 that has been displaced. CSEM is robust enough to maintain a consistent measurement over decades and has a low enough cost to allow for widespread, commercial implementation of the method.

The greatest challenge of the proposed research project was to obtain sufficient resolution at substantial depths, with any geophysical method, the deeper the target, the smaller the signals, and the smaller percentage of the survey volume that is occupied by that target. Furthermore, for large-scale surveys over deep targets the survey parameters themselves must be altered; for example lower frequencies, larger source or receiver configurations and wider station spacings, thus tending to lower spatial resolution. The ideal method for achieving the necessary spatial resolution at this depth is to move the source electrodes and receivers down boreholes and closer to the reservoir. Unfortunately, this would require arrays of dedicated boreholes, which is neither likely due to the high costs of drilling deep boreholes nor desirable as the boreholes are potential sources of leakage. Due to the unlikelihood of sites having dense arrays of monitoring boreholes, the proposed method will use a limited number of boreholes already in place, possibly a single hole, in combination with an array of surface measurements. However, one of the primary issues with using surface sources is providing sufficient signal levels at depth.

The proposed research developed and tested a robust, cost-effective sensor array for long-term monitoring of CO_2 inventories in deep geologic formations using controlled source electromagnetic methods (CSEM) to measure the electrical properties of CO_2 reservoirs. This approach drew heavily on recent advances in marine CSEM, using electrical and magnetic field signals created by transmitting electric current through borehole electrodes in or below the CO_2 reservoir. To achieve this goal, the initial task required computer models to determine survey parameters to be used to design the CSEM system. The computer models used existing information from the Ketzin CO_2 sequestration site such as well logs and earlier geophysical data. The next task implemented revisions to existing hardware. Once these tasks were complete, we conducted initial field trials to evaluate the method and suggest revisions. These revisions were used in the next (second) phase of testing hardware. The second phase also included testing of the autonomous operation. An additional assessment of the field trials was completed and a final, multiple post closure tests was conducted.

Introduction

The proposed system was designed to operate as a permanent, autonomous monitoring and data collection system that can provide much higher temporal data density than can be achieved economically with 3-Dimensional (3D) seismic surveys. It can operate over broad areas for long periods of time providing full 3D data sets on a monthly basis at a very low cost. By borrowing techniques commonly used in marine CSEM, structural information from background seismic surveys can be incorporated into the CSEM modeling to provide high resolution models of CO_2 progression within reservoirs. The system uses borehole-based vertical-electric-dipole sources placed at reservoir depths in the formation. The electric and magnetic fields induced by this source are received on the surface using an array of stations.

The project was conducted in three phases. Phase I demonstrated the feasibility of the system to collect static/reference data at the Ketzin CO_2 storage pilot site in Germany. In Phase I, numerical modeling was used to determine the optimal configurations and requirements for sensor sensitivity and data accuracy. Based on the model results, existing hardware and software were modified. The CSEM system was then field tested at the Ketzin site. The data were imaged and the results were compared with independent studies of the reservoir and overburden geo-electrical characteristics.

Phase II demonstrated the ability to provide sensitive, cost-effective measurement of changes in reservoir properties and changes in the overlying formations using a second round of measurements at the Ketzin site. A prototype autonomous recording system was developed and tested as a subset of the measurement points.

Phase III of the project quantified the advantages (and disadvantages) of the fully autonomous data collection subsystems by comparing them with repeated measurements made with mobile stations. The Phase III also provided an additional time point in measuring post-closure changes in and above the Ketzin CO_2 injection site. Validation of the CSEM field survey results were completed using a method such as other alternative and available field site data.

Phase I Studies

Numerical Modeling

Lawrence Berkeley National Lab (LBNL) and Multi-Phase Technologies, LLC conducted numerical modeling for the Controlled-source electromagnetic method (CSEM). The focus of the modeling was to determine the best array configuration and frequency that would provide the greatest sensitivity of EM signals in the CO_2 reservoir.

Numerical Modeling Methodology

The CO_2 model used a thickness of the CO_2 plume at either 20 m or 40 m with the same resistivity both set at 20 ohm-m as shown in Figure 1. Because of delays in finalizing intellectual property agreements between LBNL, MPT, and the GFZ, this model was assembled by MPT personnel from existing public data. Subsequent discussions with GFZ personnel indicated that the thickness and extent of CO_2 regions (shown as red and blue areas) are likely larger than the maximum extend of those actually created within the reservoir. However, the model should be sufficiently representative of the site to fulfill the basic goals of determining the feasibility of discriminating between changes in the reservoir near the injection point (red zone) and the larger scale movement of the CO_2 within the reservoir and to compare the magnetic and electric field approaches to delineating the reservoir signal.

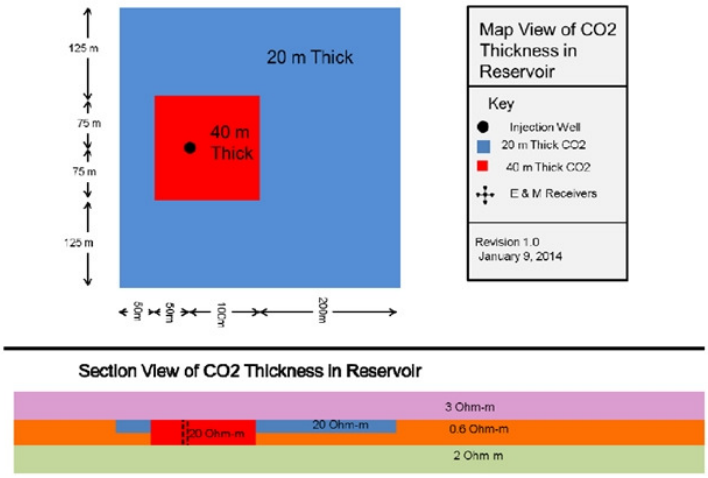

Figure 1. Plan view (top) and section view (bottom) of the CO_2 plume and reservoir. Both the red and blue areas have the same resistivity but differ in thickness (from Um, et. al, 2014).

The modeling algorithm used a 3D finite-difference, parallel 3D staggered-grid (Newman and Alumbaugh, 1995) with a layered starting model based on known layered resistivity values (as shown in the section view in Figure 1. This 3D finite-difference algorithm analyzed four different configurations:

- Model 1: Layered earth intended to model the pre-injection reservoir;
- Model 2: The current estimate of the reservoir with both the thick (red) and thin (blue) layers present;
- Model 3: Post extraction with the inner zone fully removed so the reservoir model is essentially a donut and allowing us to consider the relative sensitivity to the near and distant borehole cases; and
- Model 4: Partial extraction with a continuous 20 m thick layer.

All of the scenarios included data using 60 m source dipoles at different depths, various locations of 100 m surface receiving dipoles, and frequencies ranging from 0.125 Hz to 10 Hz. (Um et. al, 2014). Figure 2 shows an example of the numerical modeling for two plots with the source

located within the Reservoir (source depth at 650 to 710 m). The figure shows the response from the voltage (Figure 2A) and magnetic (Figure 2B) receivers located 0.5 km surface distance from the source.

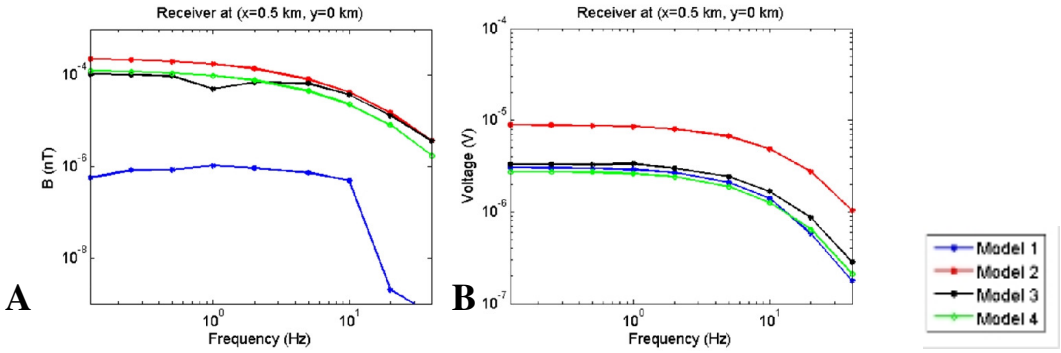

Figure 2. A) Line 1 with a Source at 650 to 710 for Ex, and B) By, and Line 1 with a Source 650 to 710 By.

Numerical Modeling Conclusions

Figure 3 shows some representative plots from the model study carried out by Um et al., (2014). All of the plots are for the surface receiver 1 km east of the injection well. The figures include plots when the 60 meter source dipole placed at a depth of 620 to 660 meters with the voltage response, Ex (Figure 3A) and magnetic response, By (Figure 3B) and the 60 meter dipole placed at a depth of 650 to 710 meters with the voltage response, Ex (Figure 3C) and magnetic response, By (Figure 3D). The figure shows the background model (no CO_2 plume) as the blue line, the current estimate of the CO_2 plume as the red line as, the "donut-shaped CO_2 plume model as the black line. and the 20 m thick CO_2 block model as the green line. The frequency range is 0.1 Hz to 1000 Hz and the receiver is placed 1 km away (x-direction). As the frequency increases, the slope of all four model curves is fairly flat; however, at above 2 Hz, the slope increases until finally sloping steeply at approximately 8 Hz. The models assumed a 1 ampere current source.

The models showed several important features. First, most of the plots the results appear to approach the steady-state asymptote for frequencies around 0.125 Hz and thus the lowest frequency data could be interpreted using the steady- state approach. Electromagnetic effects dominate the responses at about 1 Hz and over 10 Hz the amplitudes start to decrease substantially.

The electric field responses tend to be dominated by the resistivity structures closer to the borehole and thus the layered earth model (Model 1 shown as blue) and the "donut" model (Model 3 shown as black) are very similar. Changes in thickness are fairly easy to discriminate

using different source dipole locations. The electric field amplitudes are small; a few microvolts for a 1 ampere current source but should be measurable particularly if the current could be increased to about 10 amperes (Figures 3A and 3C).

The magnetic field responses tend to be more sensitive to the reservoir responses farther from the borehole and provide better discrimination between the various cases (Figures 3B and 3D). However, the amplitudes are very small, typically less than 10^{-4} nT, making them difficult to measure.

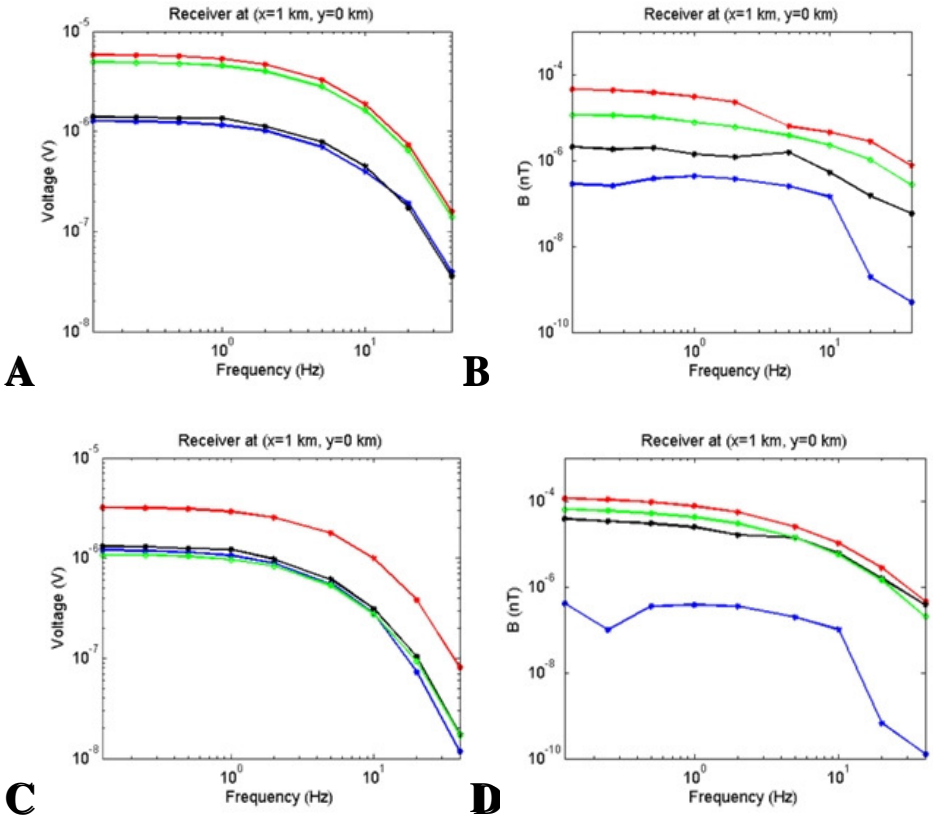

Figure 3. Line 1 with a Source at 620 to 660 A) For Ex, and B) By, and Line 1 with a Source 650 to 710 C) For Ex, and D) By.

System Modifications

Overview

The electromagnetic, resistivity, and magnetic hardware used MPT's wireless Multisource™ resistivity (MSR) data acquisition system, and conceptual electromagnetic hardware based on the techniques from marine controlled source electromagnetic methods (CSEM). The Multi-Source

distributed wireless acquisition system is designed to provide a modular platform to collect resistivity and induced polarization data. The modifications to the MSR system revolved around adapting the existing electric field measurement system to include magnetic field measurements and to modify the acquisition and processing software to deal with the new types of data. The Multisource transceivers can act either as a transmitter or a two channel receiver.

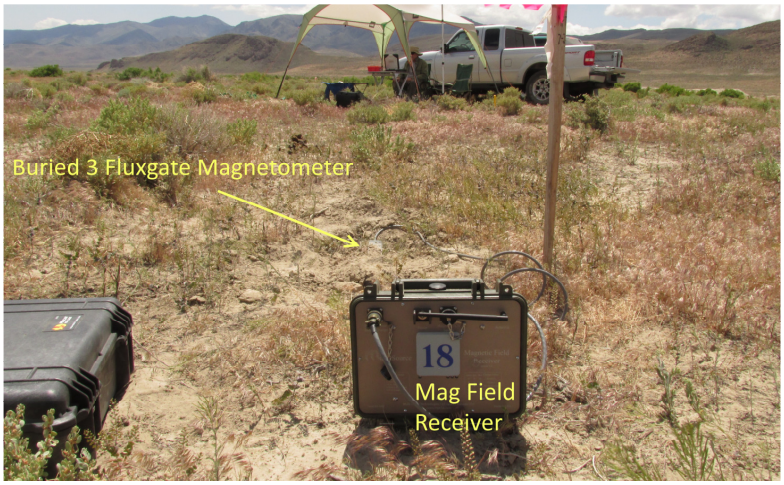

Figure 4. Magnetic Field Receiver and 3 fluxgate magnetometer.

The magnetic field sensors units contain three receiver channels, a GPS module for location and timing, a wireless module for communication, and an internal 50 watt-hour NiMh battery and battery charger. The system also provides isolated +/- 12 or +/- 15 volt power for powering external coils or fluxgate magnetometers. Figure 4 shows an example of the receiver. The fluxgate magnetometer interface contains buffer amplifiers, and buck-out circuits that provide compensation for the North and Vertical components of magnetic field.

Local Field Site Testing

MPT conducted several field tests of the magnetometers and the software for both the ERT and MMR equipment. The initial field tests were carried out to test various aspects of the magnetic and electric field receiver systems rather than collecting complete field surveys. The second round of field testing helped to refine data collection and provide information to conduct additional modification to the hardware and software. A final field test was conducted to compare the three-flux gate magnetometers (Figure 4) to low and high frequency magnetic induction coils. The single direction coils required a north, east and Z component layout (Figure 5) and required the coils to be placed in the north direction and buried under the soil.

Figure 5. Set up of the single direction magnetometer coils.

System Test Results

The initial two field tests were used solely for software and hardware development. The third field survey was used to collect ERT and MMR field data, and compare the results of the magnetic field sensors. The setting of the Astor Pass area of the Pyramid Lake Paiute Tribe (PLPT) field site provided the optimal test setting for the MPT system. The site is very quiet electromagnetically as it is relatively distant from power lines, radio towers and industrial sites. A low-noise site such as this one allowed us to evaluate the signal-to-noise levels of the sensors relatively unencumbered from background noise.

The Phoenix Geophysics MTC-80 low frequency magnetic sensors (range 400 Hz to 0.0001 Hz) and the AMTC-30 high frequency magnetic sensors (range 10,000 Hz to 1Hz) (Figure 6) used in the final field tests provided a comparable analysis to the MPT three-flux gate magnetometer.

Figure 6. The Phoenix Geophysics A) Low Frequency mag B) High Frequency mag and C) MPT three-flux gate magnetometer.

Figure 7 compares plots of the estimated standard deviations for active source measurements for magnetic-east-oriented sensor using two Bartington three-flux gate magnetometers and the low and high frequency coils. The magnetic-east orientation has essentially zero ambient fields. Using this orientation minimizes noise resulting from sensor movement in the earth's static magnetic field. In this orientation the magnetometers don't need a buck-out circuit to cancel the earth's static field. This buck-out circuit consists of a steady-state voltage that is subtracted from the output of the magnetometer to compensate for the response of the earth's static field. The buck circuits are not needed for coils which do respond directly to a steady-state field.

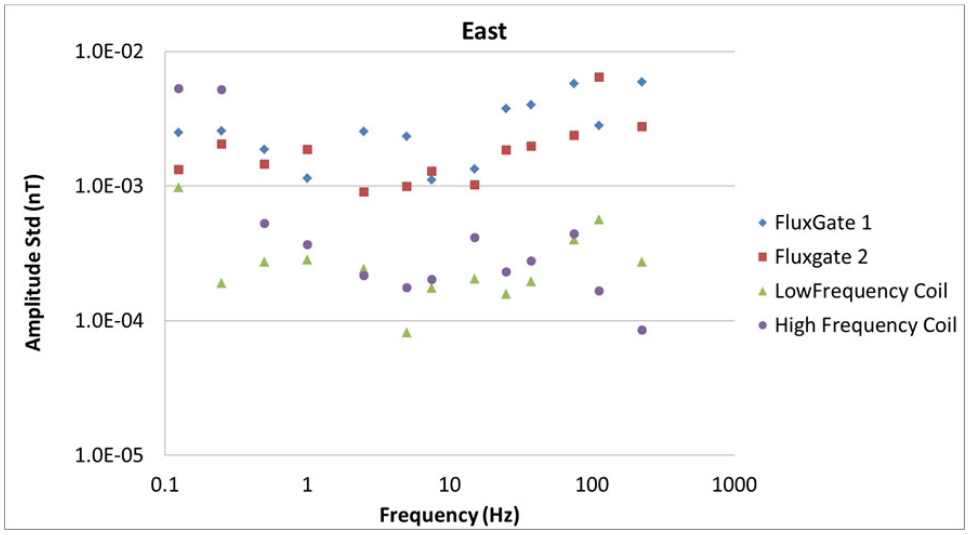

Figure 7. Data Standard Deviation from the East-oriented sensors.

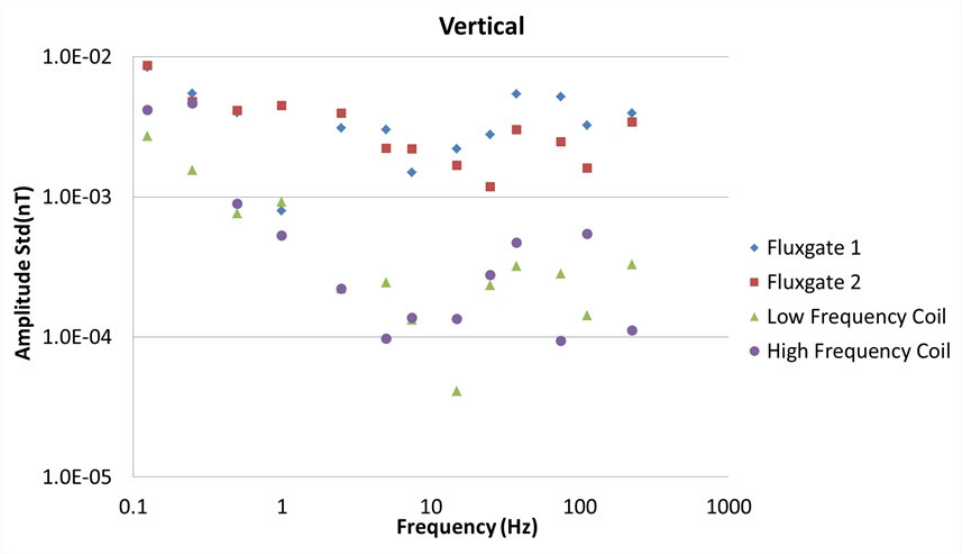

Figure 8. Data Standard Deviation from the vertical sensors.

Figure 8 shows the vertically oriented sensors of the two flux gate magnetometers and the low and high frequency coils. In northern Nevada, the vertical component of the earth's magnetic field is the largest component and thus the impact of the static fields is the largest for this component. For frequencies above 1 Hz, both the low and high frequency coil responses have standard deviations nearly an order of magnitude lower than the fluxgate magnetometers. The noise levels of the coils tend to increase as roughly the inverse of frequency at low frequencies and both the coils and the magnetometers have roughly the same noise levels around 0.1 Hz (Figure 7 and 8).

Conclusions from System Tests

Comparison of magnetometer systems showed that large, low-frequency coils could achieve better signal to noise levels than the fluxgate magnetometers at frequencies greater than 0.1 Hz. Below 0.1 Hz, the fluxgates responses are comparable to those of the coils. In addition, the fluxgates are smaller, easier to deploy, and provide a measurement of the total field, which can be used to precisely determine the deployment of the systems.

The work conducted on the hardware and software prepared the data acquisition system for the initial field testing in Ketzin, Germany. The greatest concern was the noise levels for the magnetic field measurements. Even for the coils, the measured noise levels for the coils could still be higher than the values estimated from model results. Achieving sufficient signal-to-noise levels would require increased signal averaging and increased current flow.

Phase I Ketzin Field Site Study

Overview

Field work at the GFZ CO2SINK Site near Ketzin Germany began in September of 2014. The land around the site is privately owned and all of the field operations had to be coordinated with local farmers and businesses. The original survey design followed the pattern used for ERT surveys by Bergmann et al. (2012) which used a radial pattern of receivers roughly centered on CO_2 injection well at the site. Modifications to the location, geometry, and number of sites were made. Two sites were removed from the data collection due to security issues and location to a busy road and close to a small village and walking path or located within the town near train tracks. Other sites required movement due to the train tracks or other electrically noisy issues (power lines, wind farm), or accessibility issues.

Following the initial round of data collection, the GFZ conducted a carbon extraction to simulate a rapid release that may occur in a compromised geological CO_2 reservoir. The CO_2 extraction occurred during the week of October 14, 2014, and lasted slightly over a week. Unfortunately, the amount of CO_2 removed was a small fraction of the planned extraction.

MPT conducted the follow-up trip approximately two weeks after the completed extraction campaign. The follow-up trip was to observe the short term impact of the CO_2 removal on the CO_2 saturations around the vicinity of the extraction location.

Phase I Initial Deployment

After the initial lab and local field work, revisions to hardware and software, and the preliminary model studies were conducted and assessed, the CSEM system was ready to begin the Phase I field deployment. The GFZ Ketzin CO_2 sequestration site in Ketzin, Germany was selected as the location to test the CSEM system since the site already contained ERT-equipped monitoring wells, permitted access to outlying sites and a similar testing schedule.

Figure 9. Map view of the Phase I field set up.

Data collection was carried out over a period of four days (see Table 1). In part because of the suburban nature of the survey area and in part due to limitations in the batteries used to power the system, the equipment could not be left on the remote field sites overnight. Thus the systems had to be deployed in the morning and removed each night. This was time-consuming and limited the acquisition time and the number of remote sites that could be deployed.

The Phase I field deployment set up typically included six Multisource units at the borehole (shown as a solid yellow dot in the center of Figure 9 and labeled Well 201) and three remote sites. Each remote site included; a Multisource unit, magnetometer recording unit, three-component flux gate magnetometer and three pair of Metronix magnetic coils connected to a GFZ data logger. The Metronix coils had essentially the same specifications as the Phoenix coils used in the field trials in Nevada. Figure 10A shows the typical remote site equipment design

setup. As is standard, the MSR unit and the electrodes were kept as far away from the magnetometers as possible. The typical distance from the closest electrode for the MPT magnetometer was at least 10 meters. The GFZ magnetic coils were typically placed 20 meters away from the closest electrode (Figure 10B). The fluxgate magnetometers and the GFZ magnetic coils were aligned to magnetic north and east. The magnetic horizontal fields (no vertical field) were measured with the coils as modeling indicated that the vertical component, at least from reservoir depth sources, would be unmeasurable. Although the flux gate magnetometers did not provide as good signal-to-noise levels as the Metronix coils, they were smaller and far easier to deploy. Since the magnetometers measure the static field, they are sensitive to orientation and thus provide a check on the installation. Therefore, the magnetometers were deployed at all of the sites and provided a comparison with the magnetic coil data. In addition, the Metronix magnetic coils used the signal had to be correlated with the MSR in post-processing.

The Multisource and magnetic recording units shared a tripod which held the external antennas for each device. Moving the antennas above the ground helped to extend the range of the low-power data radios used to communicate back to the control unit located near the GFZ borehole (Well 201).

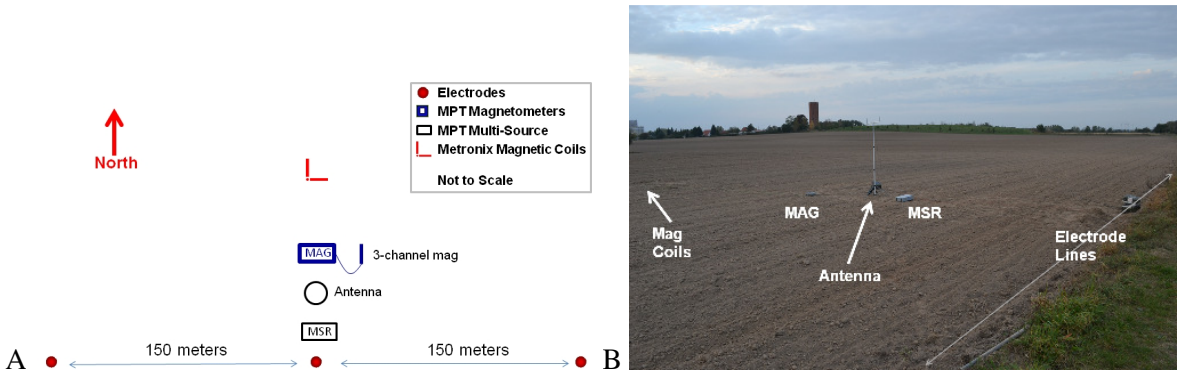

Figure 10. A) Map view sketch diagram of a typical Phase I Ketzin field survey site B) Set up of equipment at Site 12 (GFZ12A).

Table 1. Schedule for the initial Phase I field work

Date	Sites
September 26, 2014	GFZ03A, GFZ04A, GFZ05A, GFZ06A
September 27, 2014	GFZ11A, GFZ15A, GFZ16B
September 29, 2014	GFZ08A, GFZ12A, GFZ13A
September 30, 2014	GFZ01A, GFZ09A, GFZ10A
October 1, 2014	GFZ02A, GFZ06A, GFZ11A

The field campaign base included a the PC-based control unit, and the six Multisource units was placed on the GFZ Ketzin site. The six Multisource units (Figure 11 foreground) were connected to Well 201. The base site contained 15 electrodes in Well 201 and an additional 3 surface electrodes were placed near the well. Data collection commands were sent to each MSR sent via a central control module. The control module transmits the commands to each unit with compensation for timing for each unit. Data collection focused on FDIP using the frequencies from 0.125 to 37.5 Hz..

Figure 11. Six MSR units set up at the GFZ site.

In addition to MSR FDIP, MPT gathered two types of data, cross-hole ERT (XERT) data using the time-domain induced polarization mode (TDIP). The XERT survey used command and schedule files created from a previous field study conducted in 2011 by MPT and GFZ. For consistency, XERT data were collected using the time-domain IP (TDIP) mode and the same boreholes, Wells 200, 201 and 202, as in a previous field survey (which was not a part of this project). These data were used to produce percent-difference images for the NETL Phase I field acquisition (discussed later in the Borehole ERT Data section).

Phase I Post CO_2 Release Deployment

A follow up to the Phase I field work was conducted using the same electrode configuration as shown in Figure 9 with the exception of Site GFZ16B. Figure 12 shows the new field work lay out. The change to the location of the electrodes 1 and 3 at Site GFZ16B was conducted due to inaccessibility in the field (now labeled as GFZ16A). Data were collected over a period of 6 days (Table 2) and included a repeat of data collection for sites GFZ02A and GFZ06A.

Figure 12. Map view of the Follow up Phase I scattered sites field set up.

Table 2. Schedule for the Post CO_2 Release Phase I field work

Date	Sites
October 29, 2014	GFZ02A, GFZ06A
October 30, 2014	GFZ03A, GFZ04A, GFZ05A
October 31, 2014	GFZ11A, GFZ15A, GFZ16A
November 1, 2014	GFZ08A, GFZ12A, GFZ13A
November 3, 2014	GFZ01A, GFZ09A, GFZ10A
November 4, 2014	GFZ02A, GFZ06A

Data Analysis

At the onset of the survey, we knew that achieving good signal-to-noise ratios would be a challenge in the mixed industrial/farm/suburban environment of the Ketzin Site. Sophisticated signal averaging was an important part of our approach to improving signal over noise. Many of our noise sources are transient in nature. For example, the magnetic sensor coils were particularly sensitive to vehicles driving by the measurement station. A large metal object such as a car or truck moving rapidly through the Earth's natural field creates a large transient magnetic pulse on the sensors. Because of the transient nature of much of the noise, we chose to

make a series of short data measurements and then average the short runs together. The runs were weighted by the inverse of the variance of the run.

The borehole-to-surface data used borehole electrodes installed by GFZ personnel as part of a long-term monitoring project. Most of these data used relatively short, 60 m vertical dipoles. Three additional electrodes were placed on the surface to allow for long, surface-to-borehole dipoles. All of the borehole-to-surface data were collected using three units transmitting simultaneously which provided a source magnitude of about 180 ampere-meters but added considerable time to the data processing and interpretation. The primary advantage of borehole-to-surface approach was that it allowed both electric and magnetic field data to be collected simultaneously. The surveys used two types of receivers: three-component fluxgate magnetometers and Metronix coils. Previous experiments under very electrically quiet conditions showed that coil systems could produce better signal-to-noise levels, particularly at higher frequencies. However, it was not clear that the coils would retain this significant advantage over the fluxgates in a noisier suburban environment where external noise sources would likely exceed the internal noise of both types of sensors. The coils are large (1.14 m long) and heavy (about 8 kg each). Placing the coils requires that each coil is carefully aligned, leveled and buried in a shallow trench. Most of the field operation time was spent placing the coils. Placing the magnetometers was easier and quicker, as all three components were in a single package that was considerably smaller and lighter than the coils.

Figure 13 shows the amplitude responses for the Metronix coils for Site GFZ03A. This site was chosen as an example of a relatively quiet site; it was in the center of a field, away from roads, vehicle traffic, and known pipelines. It was also relatively close to Well 201, which contained the borehole-to-surface sources. In the magnetic field plots, the key indicates the uppermost transmitting electrodes used in each plot. Thus 201-1, 201-7 indicates the current source from electrodes 1 through 3 and the current return into electrodes 7 through 9. The surface electrodes are designated as 201-16 through 201-18 so data that include 201-16 as a current source or return are long (borehole-to-surface) dipoles. Because of the large transmitter moment (roughly 2000 amp meters), data points that include the surface electrodes have much larger amplitudes than those using the short borehole-only dipoles. For data with larger amplitudes, the data plots are more smoothly varying, indicative of relatively good signal-to-noise ratios. The plots for the data collected with only the deeper shorter borehole electrodes appear significantly noisier.

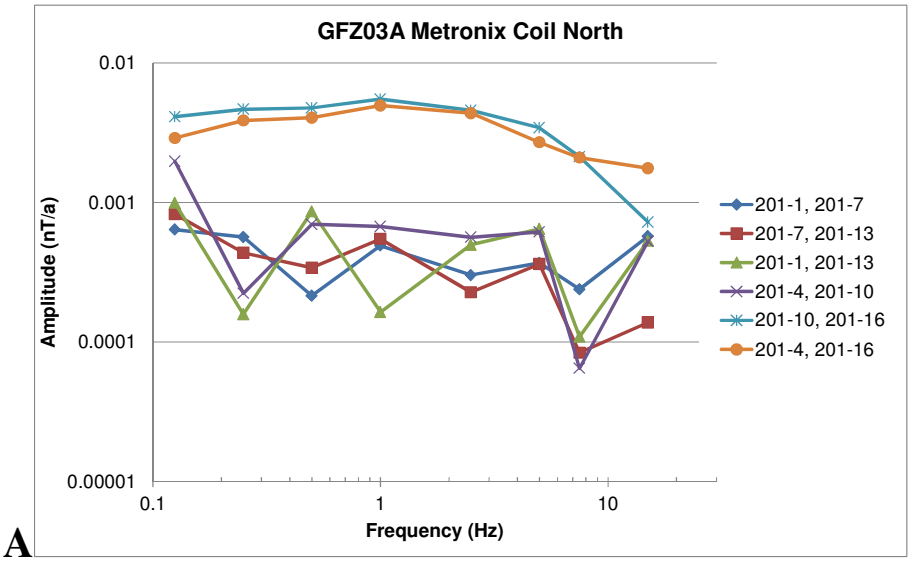

A

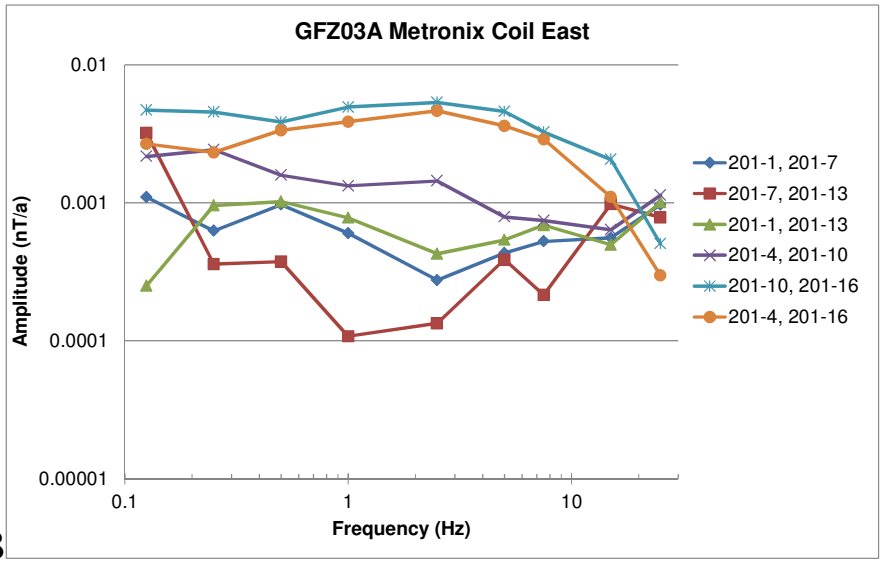

B

Figure 13. Site GFZ03A magnetic field amplitude data collected using Metronix coils for the A) North-South oriented coil and B) East-West oriented coil.

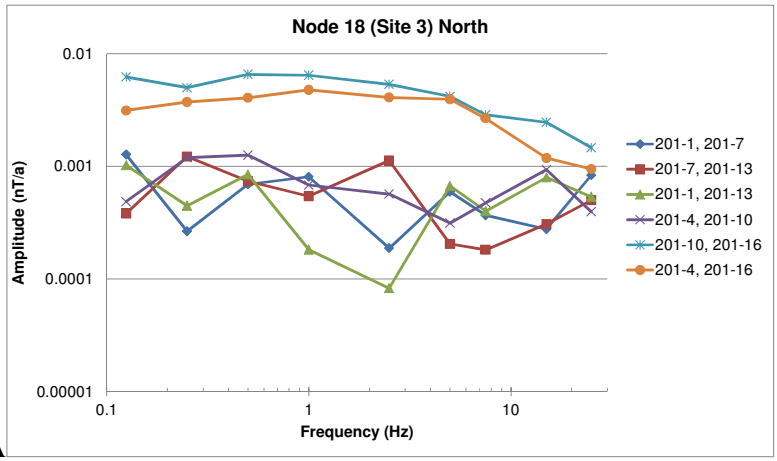

A

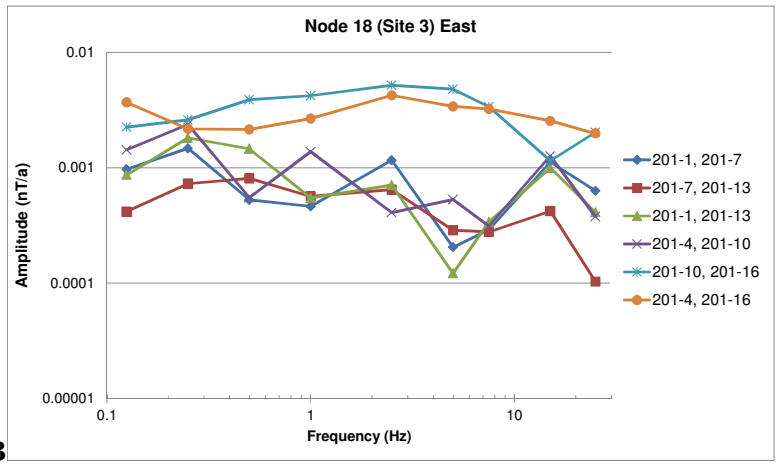

B

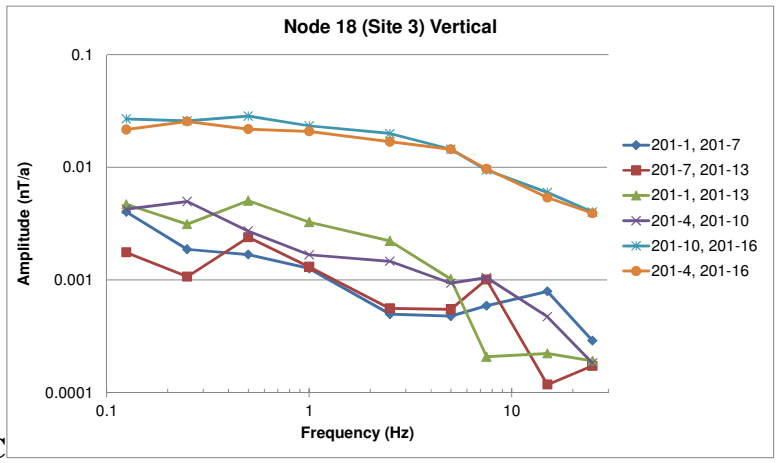

C

Figure 14. Site GFZ03A magnetic field amplitude data collected using fluxgate magnetometers shown A) the North-South component, B) the East-West component and C) the vertical field component.

Figure 14 shows the fluxgate-magnetometer data for the same stations and at the same time as the data collected with the Metronix coils (horizontal (north and east oriented)) data but also including the vertical field data. The responses for the horizontal fields are similar. For the shorter borehole-source dipoles, the fluxgate data appear moderately noisier than data collected with coils. Note that the scales are different between the horizontal and vertical field data since the amplitudes of the vertical field data are about ten times larger than those of the horizontal data.

The source of these large, anomalous vertical magnetic fields is almost certainly very shallow horizontal electric currents. A simple application of the Biot-Savart law will show that 1) if the electric currents are vertical, no vertical magnetic field response is created, 2) if the horizontal distance from the receiver to an electric current source is much less than its depth, then the horizontal magnetic fields are much greater than the vertical ones, and 3) if the vertical distance is much less than the horizontal distance than the vertical fields will be much larger than the horizontal ones. The likely source of the large vertical fields observed at this and other sites (not shown) is probably one or more shallow pipelines running through the Ketzin area.

Figures 15 and 16 show the borehole-to-surface and surface-to-borehole electric field data respectively for station GFZ03A. For the surface-to-borehole data, there was no constraint on the input current other than the limitations in power in the available equipment (375 watts) and the local contact impedance of the electrodes. Thus typical current flows ranged from 0.5 to 2.0 amps giving source dipole moments ranging from 75 to 600 amp-meters. On average, the source moment was very roughly the same for the borehole-to-surface and surface-to-borehole configurations. However, the borehole receiving electrodes are much farther from cultural noise sources, and are therefore quieter than surface receivers.

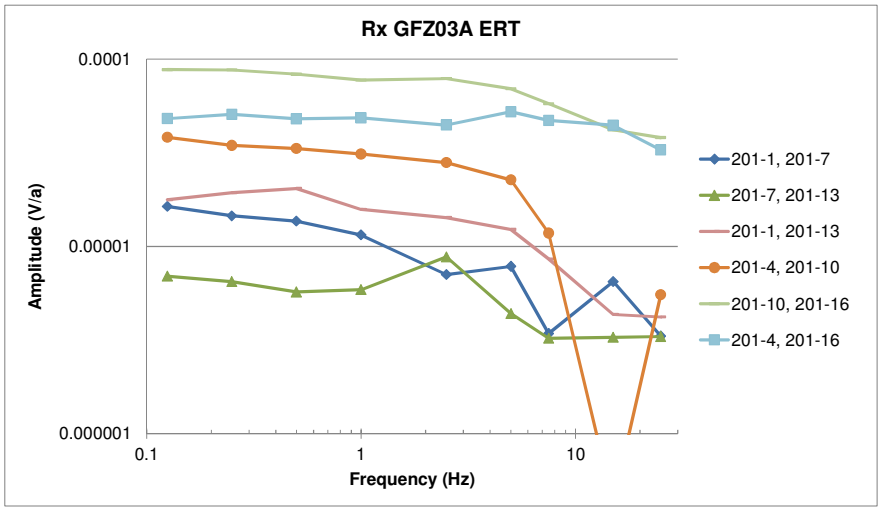

Figure 15. Borehole-to-surface electrical field amplitude data collected on October 30th, 2014 with receivers at Site GFZ03A.

Figure 16 includes a number of data points that use a combination of borehole and surface electrodes. The data have the largest amplitudes but the poorest signal-to-noise ratios. For example, the three curves with the highest amplitude show an odd glitch in the 0.25 Hz response which likely results from some cultural noise source.

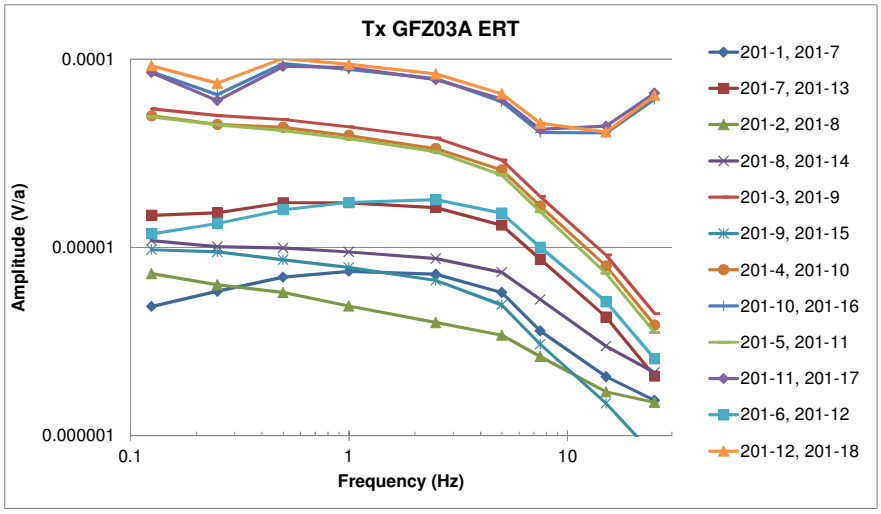

Figure 16. Surface-to-borehole electrical amplitude data collected on October 30th, 2014 with the transmitters as site GFZ03A.

XERT Data

MPT collected single and cross-borehole ERT data at the GFZ site. The single and cross-borehole data were collected in one specific command file. This file provided resistivity data between the three permanent well locations, wells 200, 201, and 202 (Figure 17). The initial Phase I trip provided a baseline data set.

The data required filtering prior to conducting an ERT inversion. MPT conducted a reciprocal percent error filter removing any reciprocal error value greater than 5%. An additional filter using geometric values greater than 5000 was applied to the data.

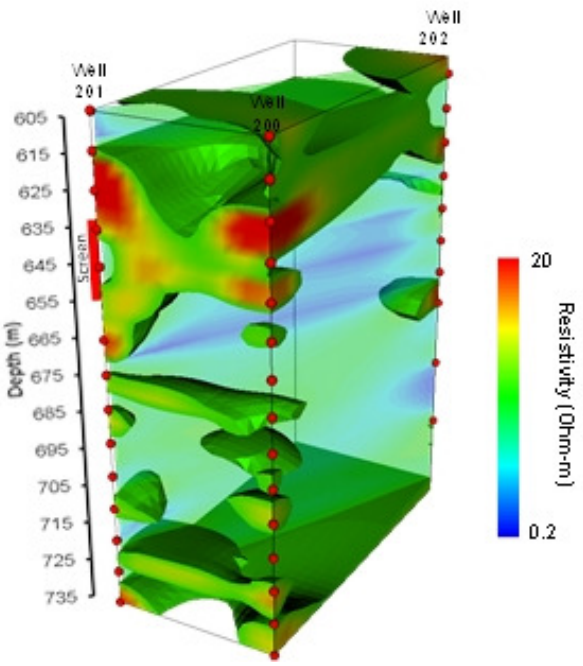

Figure 17. Perspective view of the background resistivity of the GFZ boreholes.

The ERT inversion results are shown in Figure 17. The inversion used a rho data percent error of 2% and a rho constant error term of 0.000001. Figure 17 shows the background resistivity values of the three boreholes located at GFZ. The upper portion (above 675 meters) shows the formerly injected CO_2 beginning at the screen located within Well 201 and extending to Wells 200 and 202. Figure 18 shows this extension in the cross views between Wells 201 and 200 (Figure 18A) and between Wells 200 and 202 (Figure 18B).

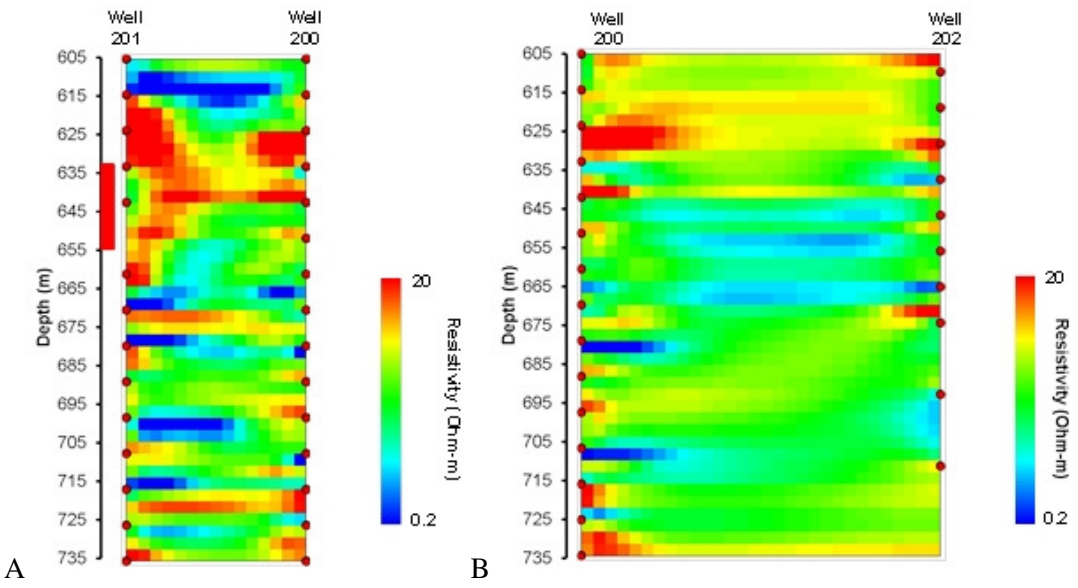

Figure 18. Cross view of the background resistivity of the GFZ boreholes for A) Wells 201 and 200 B) Wells 200 and 202.

Figure 19 displays the results of the extraction in the form of a percent-difference image. Percent-difference images show the percent change in resistivity from the background model. Additionally, percent-difference images provide a reliable estimate of changes in the formation, as well as amplifying subtle changes in the data. The percent-difference images are calculated by the percent difference between each point in the mesh. The percent difference calculation, ρ_{pdif}, is given by:

$$\rho_{pdif} = \frac{100\,(\rho_2 - \rho_1)}{\rho_1} \qquad (1)$$

where ρ_1 is the resistivity of the elements of the background model and ρ_2 is the resistivity of the elements of subsequent images.

Figure 19A shows the perspective view of the percent-difference image. The cross image plane at the screen (beginning at the depth of approximately 635 m) shows a 10% decrease in resistivity. The extent of the decrease in resistivity is relatively short when compared to cross view between Wells 201 and 200 in Figure 19B. The image plane in Figure 19B shows the decrease in resistivity extending over half the distance from Well 201 to 200.

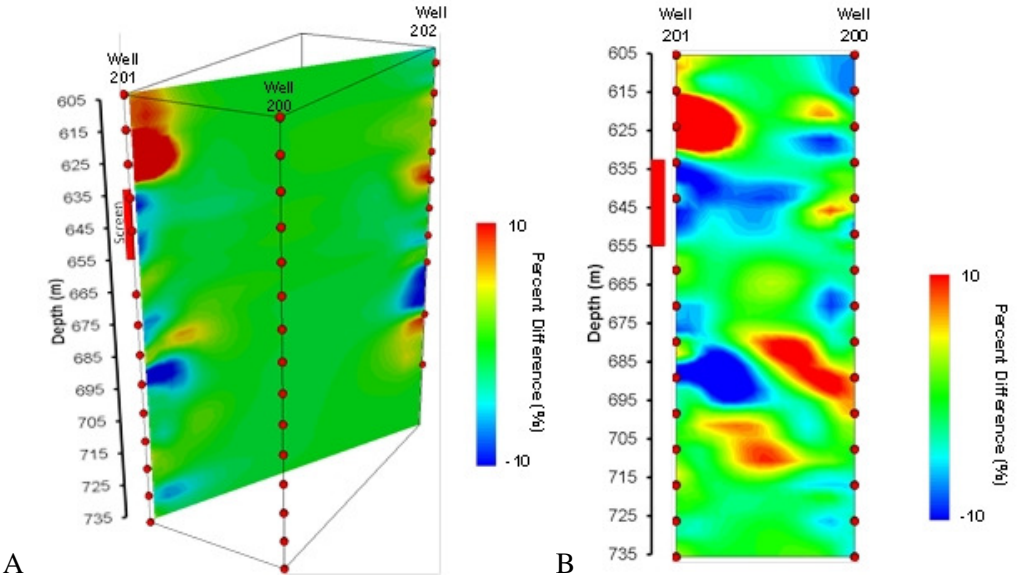

A B

Figure 19. The percent-difference images of the short-term impact of the CO_2 extraction, A) Perspective view with the image plane between Wells 201 and 202 and B) Cross view between Wells 201 and 200.

Surface-to-Borehole (STB) CSEM Inversion results

Lawrence Berkeley National Lab (LBNL) conducted several inversions on the CSEM data provided by MPT (Um, 2015). Figure 20 shows the preliminary plot of the CO_2 storage reservoir; the cross sections trend north-south and east-west. The red area indicates the CO_2 storage reservoir. This figure indicates a storage reservoir location similar to the initial background resistivity of the ERT figures (Figures 17 and 18). Figure 21 shows the cross section with a 45° rotation from the north-south and east-west cross section. Figure 22 shows the CO_2 reservoir along the XY plane at a depth of approximately 613 m.

LBNL inverted the surface-to-borehole data from select frequencies, sources and specific starting model assumptions. The starting model used a 3.33 ohm-m uniform half space. An additional starting model included a half space embedded with metal casings, unfortunately the outcome was found to provide insignificant changes to the results. The selected source frequencies used the higher frequencies 2.5, 5.0, 7.5, 15.0, and 25.0 Hz. The lower frequencies were deemed too difficult to be inverted with the LBNL code. The selected scattered site sources included in the CSEM inversion included GFZ02A, GFZ03A, GFZ05A, GFZ08A GFZ09A GFZ010A, GFZ12A, GFZ13A and GFZ14A. Issues with several of the sites not included in the inversion included incomplete data from Trip 1 to Trip 2 and modifications of the location of the

electrodes from Trip 1 to Trip 2. The inversion also considered the depth of the receivers. The depths for the receivers were placed at 640, 660, 670, 680, 690 and 700 m. Finally, since the surface-to-borehole data provided the best data acquisition results, the STB data were the only array types used for the inversion.

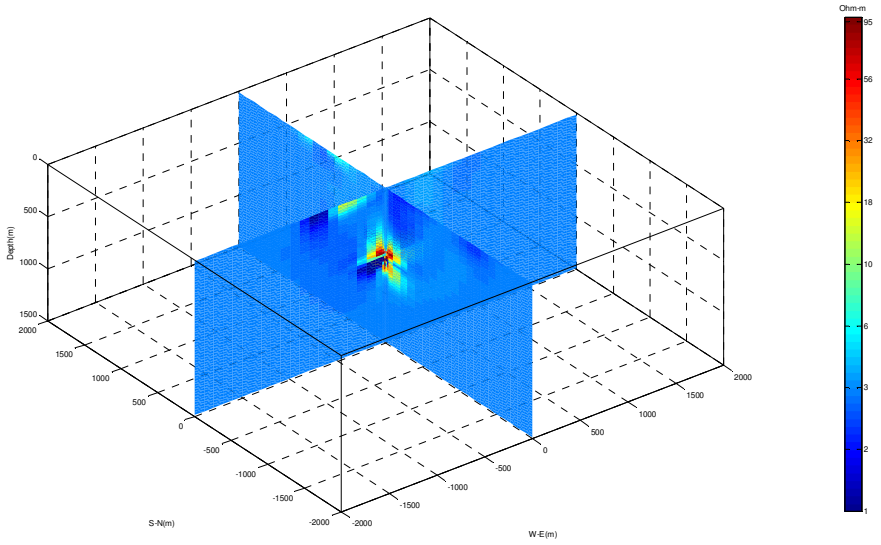

Figure 20. Perspective view of the preliminary plot of the CO_2 reservoir with the cross sections trending north-south and east-west (Um, 2015). The red area indicates the CO_2 storage reservoir.

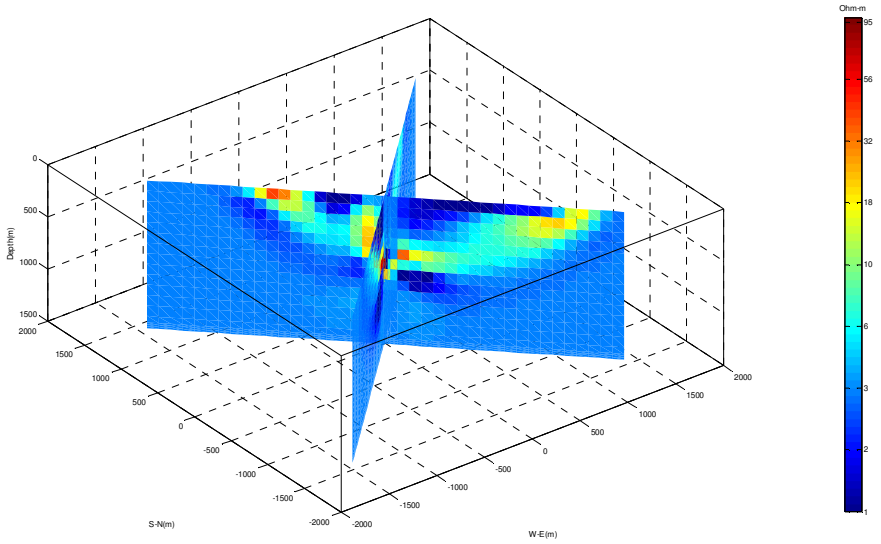

Figure 21. Perspective view of the preliminary plot of the CO_2 reservoir with the cross sections trending 45° of north-south and east-west (Um, 2015). The red area indicates the CO_2 storage reservoir.

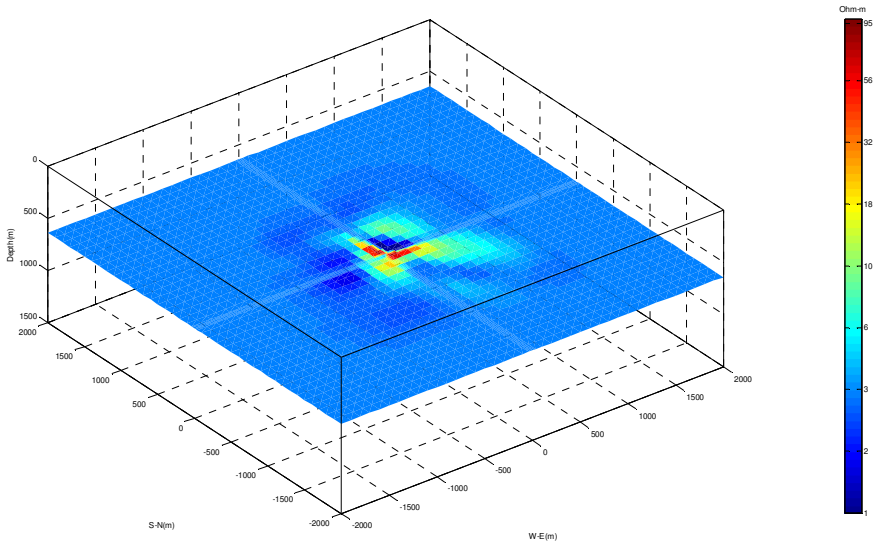

Figure 22. Perspective view of the preliminary plot of the CO_2 reservoir of the XY plane at a depth of approximately 613 m (Um, 2015). The red area indicates the CO_2 storage reservoir.

Phase I Field Studies Conclusions and Discussion

The Ketzin Site lies in mixed suburban, farmland, and industrial areas. Like similar areas in Western Europe, the Eastern United States, and many other parts of the world, the surveys need to contend with significant cultural noise. One issue is that the locations which are the easiest access for geophysical surveys are often roads with significant traffic and/or routes for regional power lines or pipelines. Near Ketzin, the best survey locations are in the center of agricultural fields in areas with virtually year-round crop production. Although the local farmers were quite cooperative, there were schedule conflicts and these areas would not be useable for permanent monitoring locations.

Of the types of data collected, the surface–to-borehole data had the best signal-to-noise ratios and was thus most amenable to collection in this environment. The magnetic field data were the most severely impacted by cultural noise including both electrical and the impact of conductive structures such as pipelines. The magnetic data also required the most expensive equipment and were the most expensive to collect. Metronix Magnetic coils used a separate data acquisition system and required additional data processing to synchronize results with the MPT three gate flux magnetometers. Several sites were not conducive to magnetic data acquisition (i.e. next to high traffic roads or railroad tracks) and the sites were either removed or placed in a different location. The initial plan required MPT to set up four sites daily, however, additional set up time was needed to set up the Metronix magnetic coils. The set up time doubled when using the magnetic coils. Therefore, MPT scaled back the collection from four to three sites daily.

The LBNL STB CSEM inversion required 25 minutes per inversion iteration with 6561 MPI processes (NERSC Edison). The images appear to be able to detect the reservoir and show roughly the correct location and direction of CO_2 movement

A major goal of the following project phases was to improve the resolution of the reservoir by concentrating on the surface-to-borehole data and increasing the density of transmitting locations.

Phase II, III Studies

Phase II, III Field Array Modifications

One of the final experiments carried out by the GFZ was controlled brine injection in January 2016. The brine solution should have had a resistivity similar to the background resistivity of the reservoir (approximately 3.8 ohm-m). The goal was to displace CO_2, creating a decrease in resistivity around the injection well.

Because the previous CO_2 release experiment only created small changes in the reservoir, it was felt that the break between Phase I and the final Phase II and Phase III surveys provided an opportunity to revise the survey design and to target the monitoring the reservoir changes due to this final experiment.

As discussed earlier in this report, much of the field acquisition time was spent deploying magnetic sensors which produced little interpretable data in this environment. The magnetic field data appear to be particularly vulnerable to interference from pipelines (as shown by the large values of the vertical fields) (Figure 23). The Phase II field work focused on MPT's collection of electric field data using the MSR data acquisition system, the MPT DAS-1 and the newly developed autonomous Multisource system. Excluding magnetic field data allowed us to substantially increase the number of simultaneous remote stations and thus to deploy a high density surface arrays (Figure 24). This array places three lines trending north-south along roads and easy access areas. The array uses 69 surface electrodes with 150 meter spacings and includes electrodes in the Well 201 borehole.

Where possible, the high density surface array places most of the surface electrodes away from the gas pipelines (GTPro Geotechnologie GmbH, 2012). Lines 1 and 3 cross the gas lines with a minimal number of electrodes near the gas lines, however Line 2 electrodes are near the gas lines. The high density surface array provided a better signal-to-noise ratio and therefore improved the data quality.

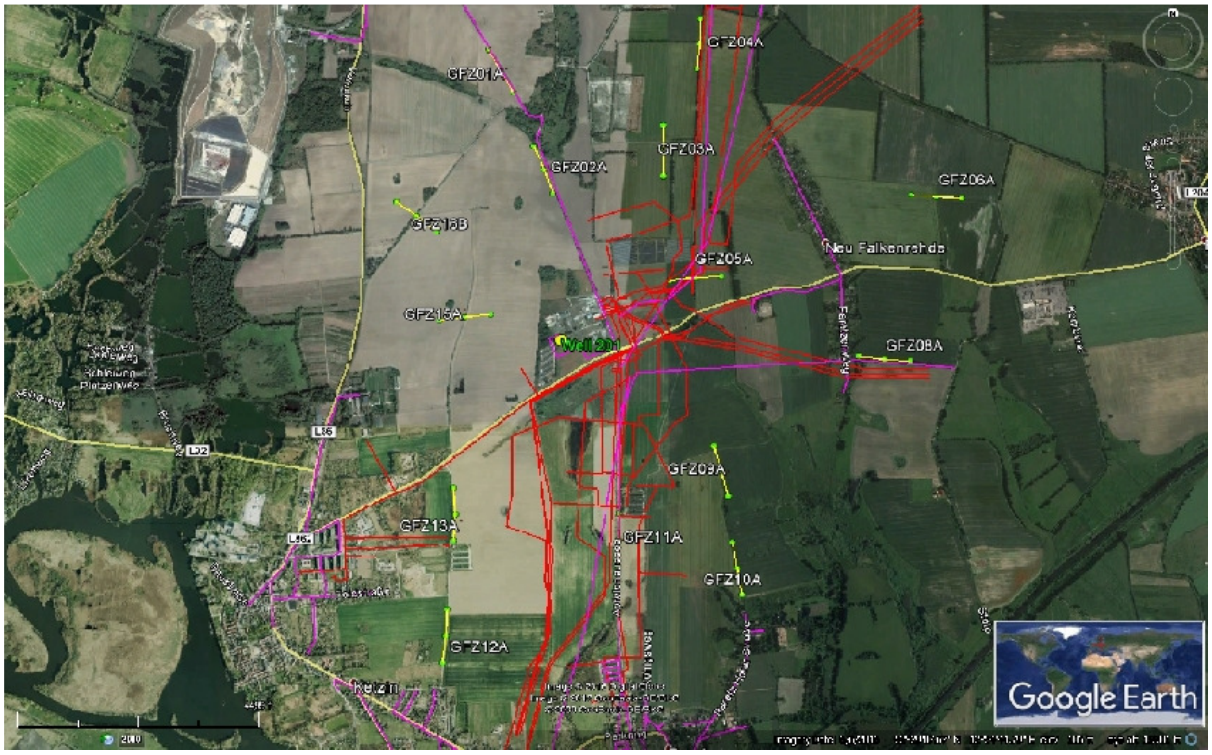

Figure 23. Map view of the Phase I scattered sites field set up and gas pipeline.

Figure 24. Map view of High density MSR set up and gas pipeline.

Hardware Modifications and Design for Autonomous System Operation

Autonomous System Operation and Set Up

One advantage of electrical methods is that they are highly amenable to autonomous operation. MPT deployed two autonomous receiving units at the Ketzin site. As the site is located in a suburban area, using receiving units in a borehole-to-surface configuration was chosen to eliminate the possibility of local inhabitants contacting live transmitter cables. The hope was that using autonomous operation would allow long periods of data averaging to overcome the inherent signal-to-noise limitations of the borehole-to-surface method. Figure 25 shows the locations of the autonomous units. The requirements for the placement of the autonomous units included placing the units in a secure and disturbance-free area that provided clear communication with the command module at the GFZ communications shed and the ability to provide representative data of the CO_2 storage reservoir.

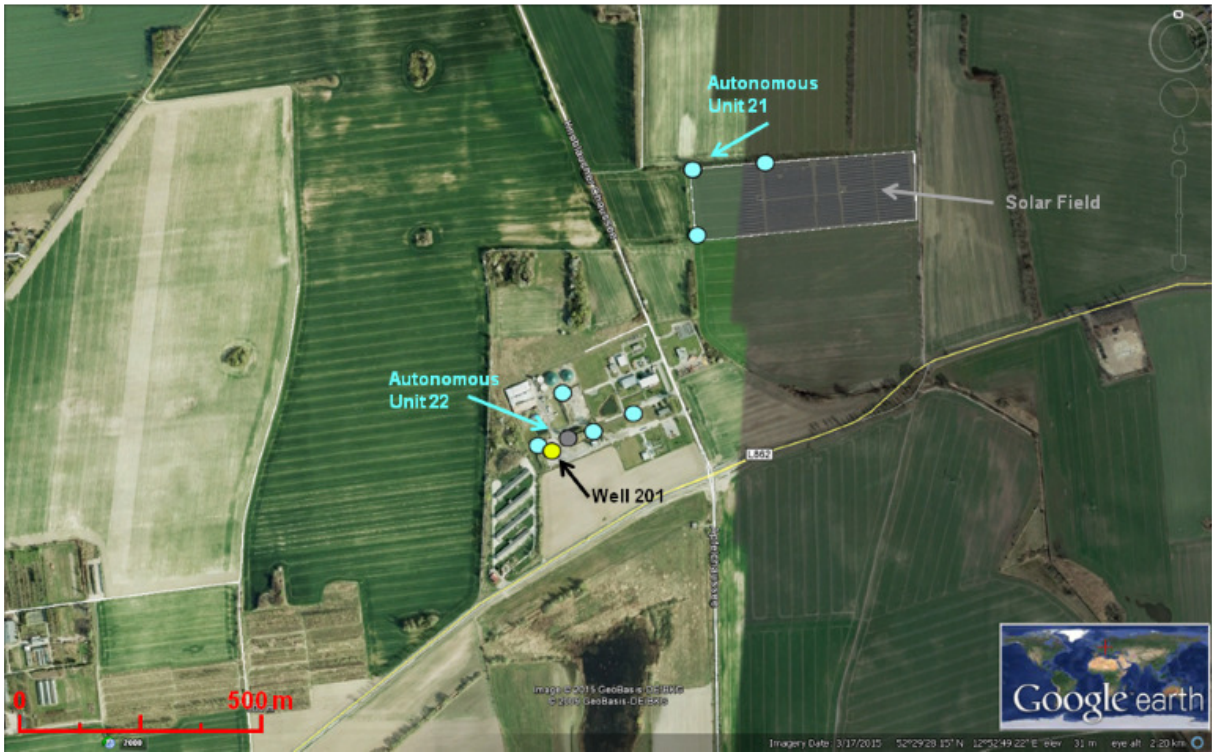

Figure 25. Placement of autonomous units

GFZ provided MPT an area to place one of the autonomous units (Unit 22) within the secured and fenced location containing the wells for the carbon sequestration study. Figures 26A and 26B show the Unit 22 set up within the secured GFZ area. MPT placed the autonomous unit on

an embankment next to the communication shed. The placement of the unit provided the optimal location of collecting sunlight for the greatest length of time. The location is free of any obstructive shadow that would affect the amount of sunlight reaching the solar panels. The Unit 22 receiving electrodes are placed in an approximate "T" pattern (shown as light blue dots in Figure 25) and surround Well 201. The placement of the electrodes required MPT to place the wires either within a protective plastic cable protector or along the fence to prevent landscaping staff from accidentally cutting the wires.

Figure 26. Unit 22 located within the GFZ fenced area A) front view B) site view with Well 201 in the background.

Placing autonomous units was placed in the surrounding countryside proved to be difficult since secure locations were very limited. However, GFZ's Mr. Schuster located a secured solar field area where the owner, allowed MPT permission to place a unit within the fenced solar field area on the condition that any equipment cannot place a shadow on the existing solar panel. Figure 25 shows the map location of the solar field and Unit 21 relative to both Well 201 and Unit 22. Figure 27 shows autonomous Unit 21 set up within the secured solar field area. MPT placed the autonomous unit on a fence post on the north side of the solar field. The fence post was over 2 meters in height and allowed the solar panel to be placed at a maximum secured height to prevent any shadows from obstructing the amount of sunlight reaching the solar panels.

The Unit 21 electrodes are placed in an approximate "L" pattern (shown as light blue dots in Figure 25). The fence restricted the electrode placement within the solar field.

An issue arose for the long term autonomous survey. Since the borehole arrays were committed for ongoing monitoring by the GFZ, the time available for the autonomous system monitoring was restricted. The system became available for data collection on February 18, 2016. MPT conducted a series of basic checks including communication between the field computer and the data acquisition system. Several issues arose during the initial test run and these issues were not fixed until March 1, 2016. Unfortunately, one of the autonomous units failed to function normally. It was later determined that a faulty electrical component caused the failure in Unit 21. Data collection on Unit 22 was restricted to daylight hours as the solar panels were not able to charge the batteries during the winter months. Therefore, the data from the autonomous units were limited and are not included in the Phase III field acquisition results.

Phase II Field Studies at the Ketzin Site

Figure 27. Unit 21 located within the fenced area of the solar panel farm.

MPT collected data in s frequencies, from 0.125 Hz to 37.2 Hz and used dipole and Walsh arrays in the high density Multisource configurations. The data used the GFZ borehole and eight remote sites per data run. The data used reciprocity for quality assurance checks.

The high definition Multisource arrays followed known areas of public right-of-ways or areas of the owner-permitted land. MPT made an effort to place Multisource units in previously remote sensor locations, however in order to conduct a uniform spacing of 150 meters between each electrode line, the previous sensor locations may not have lined up with the spacing and was modified. Table 3 shows the data collection schedule of the field work. The borehole (Well 201) was used throughout the entire project and is not listed in the table.

Table 3. Schedule for the initial Phase II field work

Date	Sites
August 26, 2015	Survey of Line 3 MSR sites
August 27, 2015	Data collection for Line 3
August 28, 2015	Data collection for Line 3, Survey of Line 2
August 29, 2015	Data collection for Line 2
August 31, 2015	Data collection for Line 2
September 1, 2015	Data collection for Line 1
September 2, 2015	Placement of autonomous receiver system at Well 201
September 3, 2015	Placement of autonomous receiver system at solar field

Data collection began on August 27, 2015. MPT and GFZ staff surveyed Line 3 the previous day of data collection. Due to scheduling conflicts with the farmers in the area of interest for Line 3, data collection for this line became the priority. Areas for Lines 1 and 2 were available throughout the project period and data collection could be conducted at any time during deployment. Line 3 data collection spanned over two days, from August 27 to 28. Day 1 data collection consisted of FDIP line tests using a frequency range of 0.125 Hz to 1 Hz including IP. Day 2 collected data from Line 3 using dipole and Walsh arrays 0.125 Hz to 37.5 Hz. The dipole arrays used long dipoles only.

Data collection for Line 2 began on August 29 and August 31. Day 1 data collection consisted of FDIP line tests using a frequency range of 0.125 Hz to 7.5 Hz. Day 2 collected data from Line 2 using dipole and Walsh arrays 0.125 Hz to 7.5 Hz.

During data collection of Line 2, MPT staff began site surveys for the final line, Line 1. Data collection for Line 1 began on September 1, 2015. The data collection consisted of FDIP line tests using a frequency range of 0.125 Hz to 7.5 Hz using dipole and Walsh arrays.

Phase III Field Studies at the Ketzin Site and Acquisition Results

On April 4 to April 12, 2016, MPT conducted the Phase III CSEM and the surface multi-source resistivity (MSR) field study in Ketzin, Germany. The Phase III field work used MPT's wireless Multisource™ resistivity (MSR) data acquisition system and the recently developed autonomous MSR system. This trip was the final field campaign of the CSEM field study.

The Phase III field campaign used the same placement for the electrodes as Phase II (Figure 24). As with the Phase II field campaign; the Phase III field set up placed surface electrodes as far away from near-surface gas pipelines, as practicable.

Table 4 outlines the data collection arrays and frequencies for Phase III. The table includes September 4, 2015 (the date for installation of the autonomous units) since Phase III included autonomous data collection.

April 9 and 11th provided MPT with the ability to repeat Lines 1 and 2 respectively. The repeated data collection provided a complete data acquisition for these lines.

Table 4. Schedule for the initial Phase III field work

Date	Sites	Arrays	Frequency
September 4, 2015	Collect autonomous unit data until April 4, 2016		
April 5, 2016	Survey in Line 1	FDIP dipole, linear and Walsh	0.125 Hz to 7.5 Hz
April 6, 2016	Data collection for Line 1, Survey of Line 2	FDIP linear, dipole and Walsh	0.125 Hz to 7.5 Hz
April 7, 2016	Data collection for Line 2, Survey of Line 3	FDIP linear, dipole and Walsh	0.125 Hz to 7.5 Hz
April 8, 2016	Data collection for Line 3,	FDIP linear, dipole and Walsh	0.125 Hz to 7.5 Hz
April 9, 2016	Data collection for Line 1 (2^{nd} run), run cross borehole ERT	FDIP linear, dipole, Walsh and Cross-Borehole data including short dipole, horizontal and cross borehole	0.125 Hz to 7.5 Hz
April 11, 2016	Data collection for Line 2 (2^{nd} run)	FDIP linear, dipole and Walsh	0.125 Hz to 7.5 Hz

Table 5 shows the electrode pair configurations within Well 201. The configurations are the same as the Phase II field campaign; however, the electrode numbering scheme changed in Phase III, including a change to the Well 201 surface electrode from electrode number 16 to electrode number 1. This change was made to reflect the naming convention used by GFZ, which numbers the shallow-most electrode as 1 and the deepest electrode as 15.

Table 5. Electrode Pair settings in Well 201

Transmitting Electrode Pairs	Location (depth (m))	Distance (m) between electrodes
Electrodes 7, 13 and Surface (“01”)	Elec. 7 at -610.1, Elec. 13 at -669.5, Elec. “01” (surface) at 34	Between Electrodes 7 and 13 = 59.4 Electrodes 7 and Surface = 644.1
Electrodes 1,7 and 13	Elec. 2 at -562.48 Elec. 8 at -621.35, Elec. 14 at -679.48	Between Electrodes 2 and 8 = 58.87 Electrodes 8 and 14 = 58.13

Phase II, III Data Analysis and Modeling

The data analysis from the Phase III data acquisition provided images of the CO_2 reservoir after the brine injection with focus on the 0.125Hz data using the direct current (DC) code ERTLab64™.

Figure 28 shows the revised inversion for the Phase II field campaign. The cell (voxel) size is 15 m (x-direction) by 15 m (y-direction) by 10 m (z-direction). Due to limitations on computer memory processing required a large cell size, overall 3.24 million nodes and 3.17 million cells (voxels) made up the full mesh size. The high resistivity (red) area appears to correspond to the extent of the CO_2 plume in the reservoir. The horizontal plane (Figure 28A) is shown at a depth of 635 m below the surface. This is the known location of the CO_2 plume. Additional red dots represent locations of surface electrodes. The x-direction cross section A-A' (Figure 28B) shows the CO_2 plume through the injection well (bottom red line). The CO_2 plume appears to be thickest (approximately 90 m) around the well and tapers off in an asymmetric pattern away from the well. Most of the plume appears to flow to the left (west) of the well. The y-direction cross section B-B' (Figure 28C) shows the CO_2 plume through the injection well (bottom red line). The CO_2 plume again appears to be thickest (approximately 90 m) around the well and tapers off in a symmetric pattern away from the well. Although the plume appears to flow symmetrically away from the well, there is slightly more movement to the left (north) of the well. Further away from the injection well, the resolution is lower and the anomaly will appear to be more spread out.

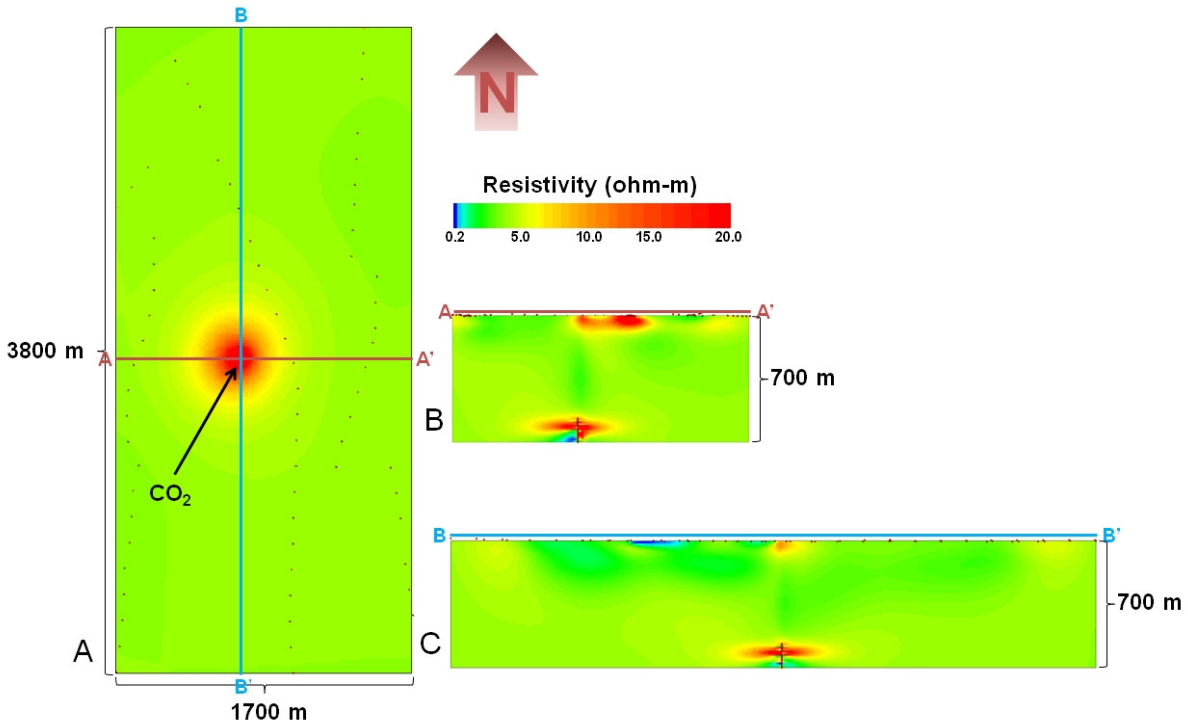

Figure 28. The data analysis of the Phase II data from the high-density array shows the extent of CO_2 in the reservoir in a A) horizontal plane at a depth of 635 m, B) the x-direction cross section A-A' through the injection well and C) the y-direction cross section B-B' through the injection well. The model scale uses a Log 10 scale.

Figure 29 shows the perspective view of the resistivity from the data analysis. The perspective view includes the same dimensions as the map view in Figure 28 (3500 m by 1700 m). The cross sections along the x and y-axes highlight the location of the CO_2 plume (10 to 20+ ohm-m). The x-direction cross-section bisects the injection well; however, the y-direction cross section is offset 50 m east from the injection well to highlight the plume morphology.

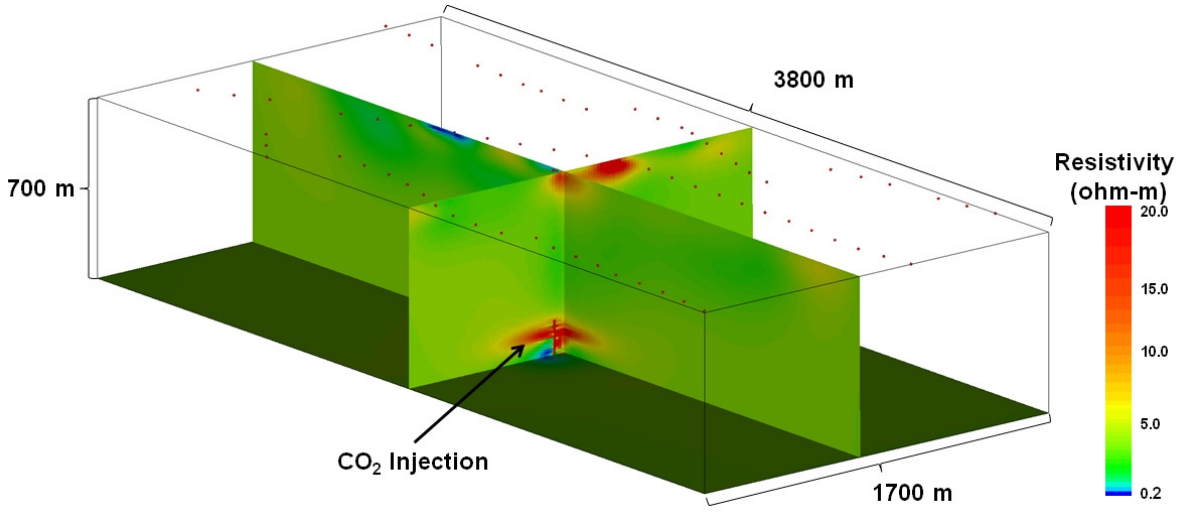

Figure 29. Perspective view of the CO_2 plume from the Phase II field campaign. The results use a Log 10 based color scale.

Figure 30 shows the inversion for the Phase III field campaign that began in April 2016 after the brine injection. The red area shows the extent of the CO_2 plume in the reservoir. The mapped horizontal plane (Figure 30A) represents the plane at a depth of 635 m below the surface. This is the known location of the CO_2 plume. The plume appears to be larger than the Phase II map view. The x-direction cross section A-A' (Figure 30B) shows CO_2 plume through the injection well (bottom red line). The CO_2 plume appears to have expanded, from approximately 90 m in Phase II to approximately 110 m in Phase III, around the well and tapers off in an asymmetric pattern away from the well. The plume appears to preferentially flow to the left (west) of the injection well. The y-direction cross section B-B' (Figure 30C) shows CO_2 plume through the injection well (bottom red line). The CO_2 plume appears to taper off in a symmetric pattern away from the well and appears to have an increased flow to the right (south) of the well.

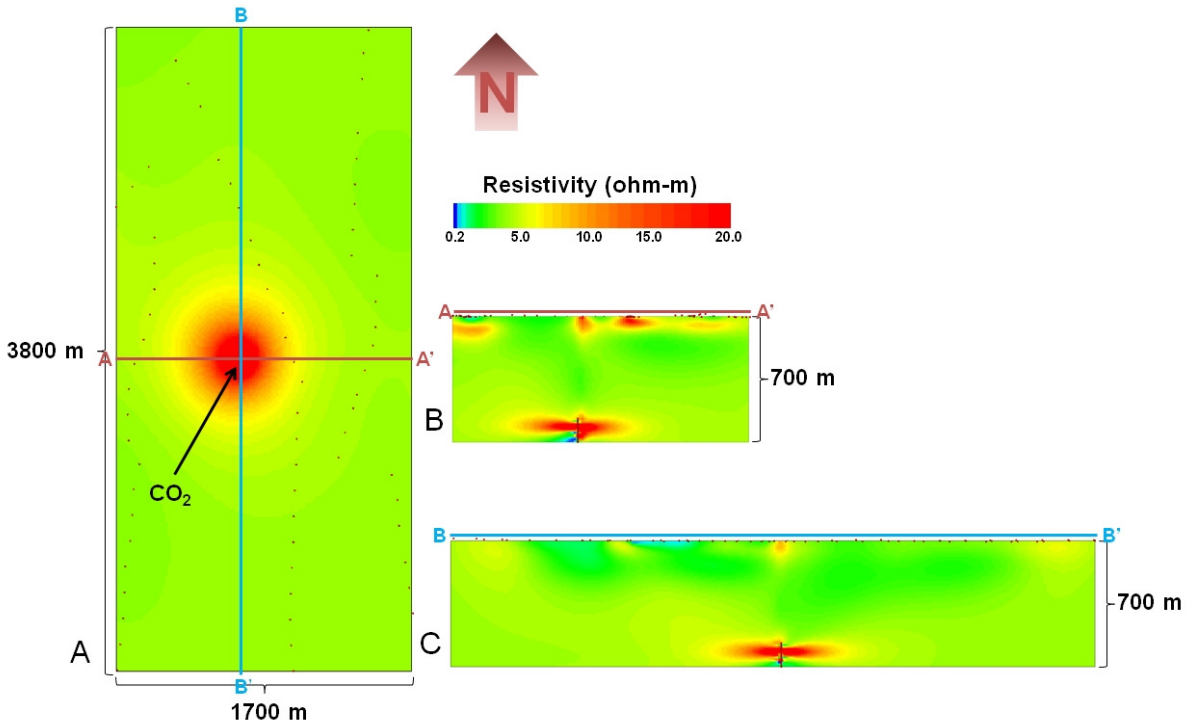

Figure 30. The data analysis of the Phase III data from the high-density array shows the extent of CO_2 in the reservoir in a A) horizontal plane at a depth of 635 m, B) the x-direction cross section A-A' through the injection well and C) the y-direction cross section B-B' through the injection well. The model scale uses a Log 10 scale.

Figure 31 shows the perspective view of the resistivity from the data analysis using the new well location. The perspective view includes the same dimensions as the map view in Figure 30 (3500 m by 1700 m). The cross sections along the x and y-axes highlight the location of the CO_2 plume (10 to 20+ ohm-m). The x-direction cross-section bisects the injection well; however, the y-direction cross section is offset 50 m east from the injection well to highlight the plume morphology and the increase in size.

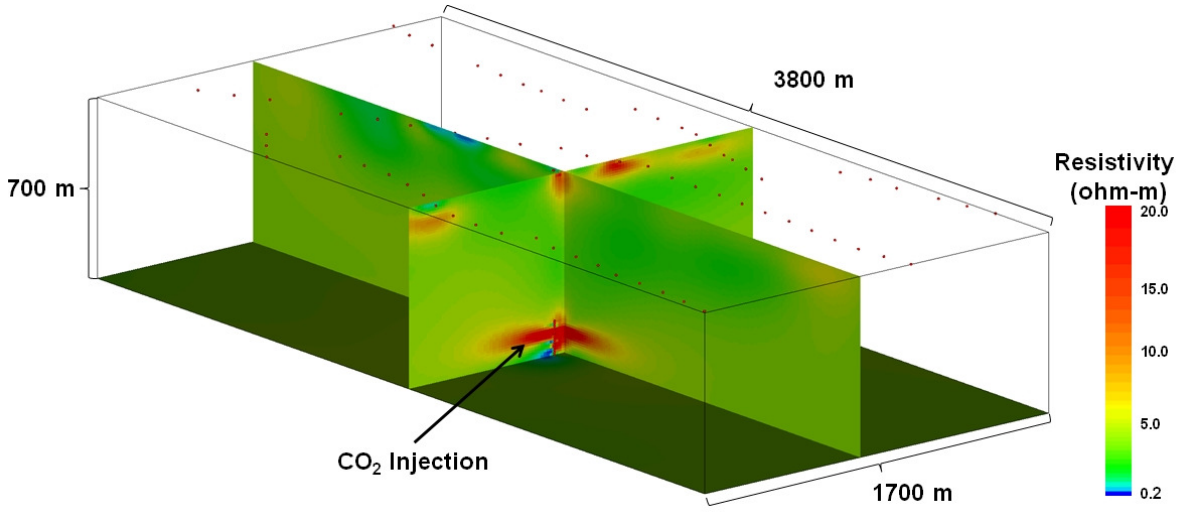

Figure 31. Perspective view of the CO_2 plume from the Phase III field campaign. The model scale uses a Log 10 scale.

Overall, there appears to be an increase in resistivity of the CO_2 plume from the Phase II field campaign to the Phase III field campaign. This increase appears to be counterintuitive to the known field activity that occurred between the Phase II (September 2015) and Phase III (April 2016) campaigns.

To highlight this effect, we created an image of the absolute resistivity change between Phase II and Phase III. Using the ERTLab64™ Viewer's absolute resistivity function, the following equation was used for each voxel in the Phase III model to the Phase II model,

$$Absolute\ change\ in\ resistivity = Phase\ III\ - Phase\ II \quad (1)$$

Where Phase III is the voxel value of the Phase III inversion model and Phase II is the corresponding voxel value of the Phase II inversion model.

Figure 32 shows the results of the absolute change in resistivity between the Phase II and Phase III field campaigns. The figure shows significant change around the injection area. At 635 m depth (Figure 32A) there is an overall increase in resistivity around the borehole. The increase circumscribes the borehole close to the injection point; however, there is a decrease in resistivity at the borehole injection points that extends approximately 30 m from the borehole. Figure 34 shows a close up of the map view area.

Figure 32B shows the x-direction cross section A-A' of the absolute change in resistivity through the injection well (bottom red line). The increase in resistivity appears to be thickest near the right side (east) of the well (approximately 50 m) and extends approximately 60 m east. To the

left (west) side of the borehole, there is an increase in resistivity approximately 10 m thick and extending asymmetrically approximately 75 m from the borehole. Figure 35 shows a close up of the A-A' cross section at the borehole.

Figure 32C shows an increase in resistivity extending north and south from the borehole. The increased change in resistivity on the right (south) of the borehole extends approximately 90 m from the borehole. The left (north) side of the borehole also shows an increase in resistivity approximately 60 m thick and extending asymmetrically from the borehole. However, there are intermittent decreases in resistivity around the borehole, most notably from the borehole injection point. The decrease in resistivity appears near and on the borehole from near the top of the well to the middle of the well. Figure 36 shows a close up of the B-B' cross section at the borehole.

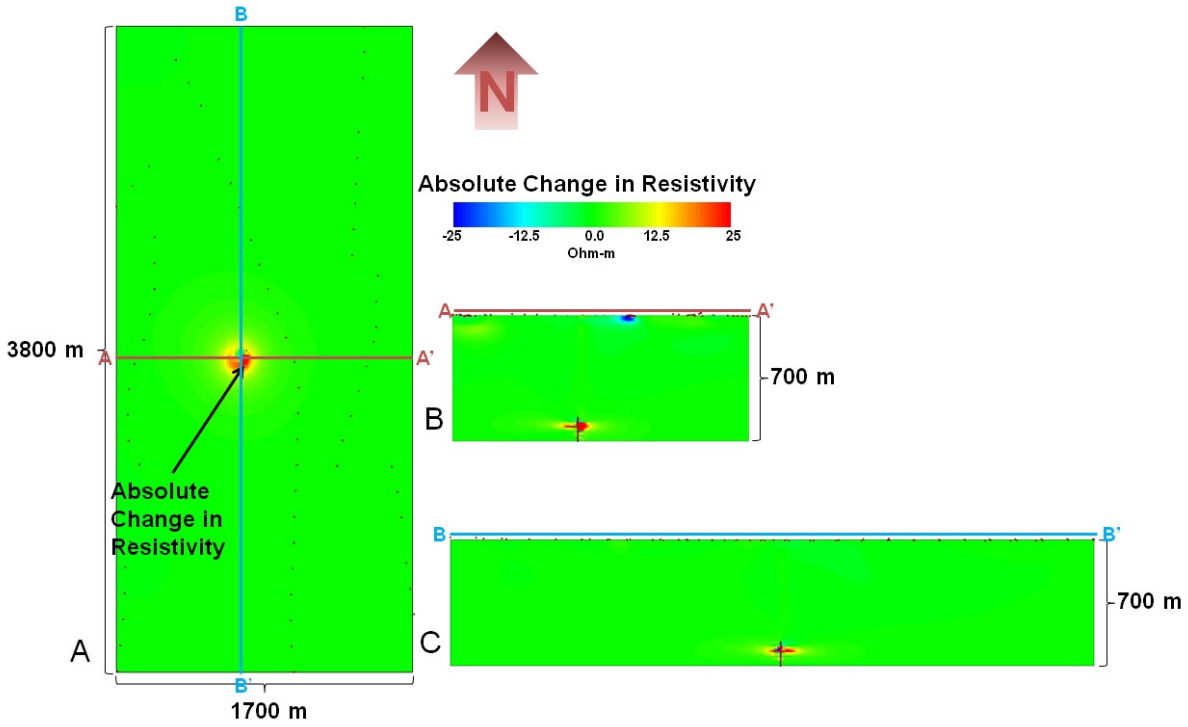

Figure 32. The absolute change in resistivity between Phase II and Phase III field campaigns are highlighted in the reservoir in a A) horizontal plane at a depth of 635 m, B) the x-direction cross section A-A' through the injection well and C) the y-direction cross section B-B' through the injection well. The model scale uses a linear scale.

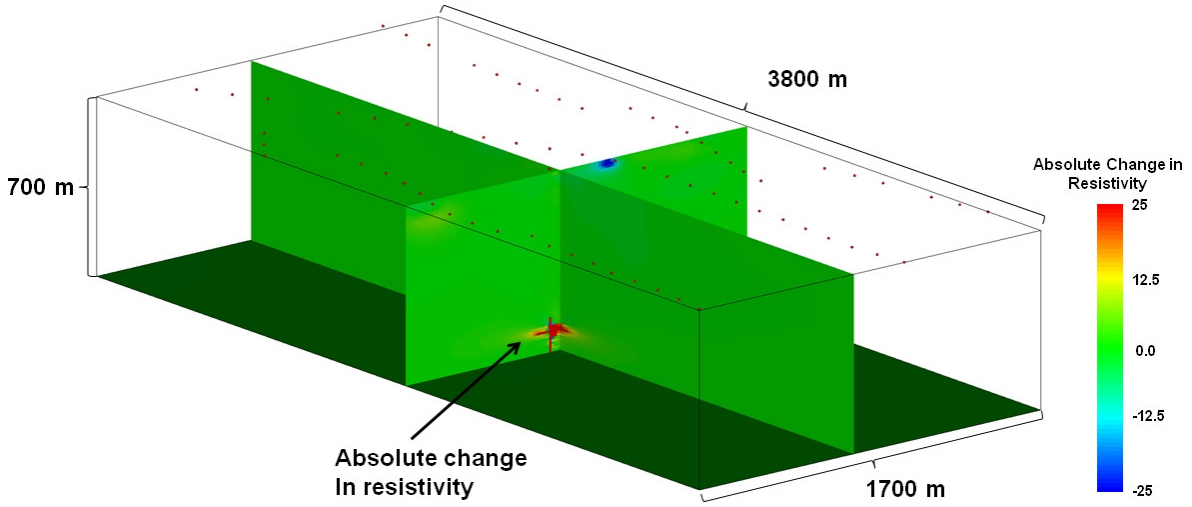

Figure 33. Perspective view of the absolute change in resistivity from the Phase II and Phase III field campaigns. The model scale uses a linear scale.

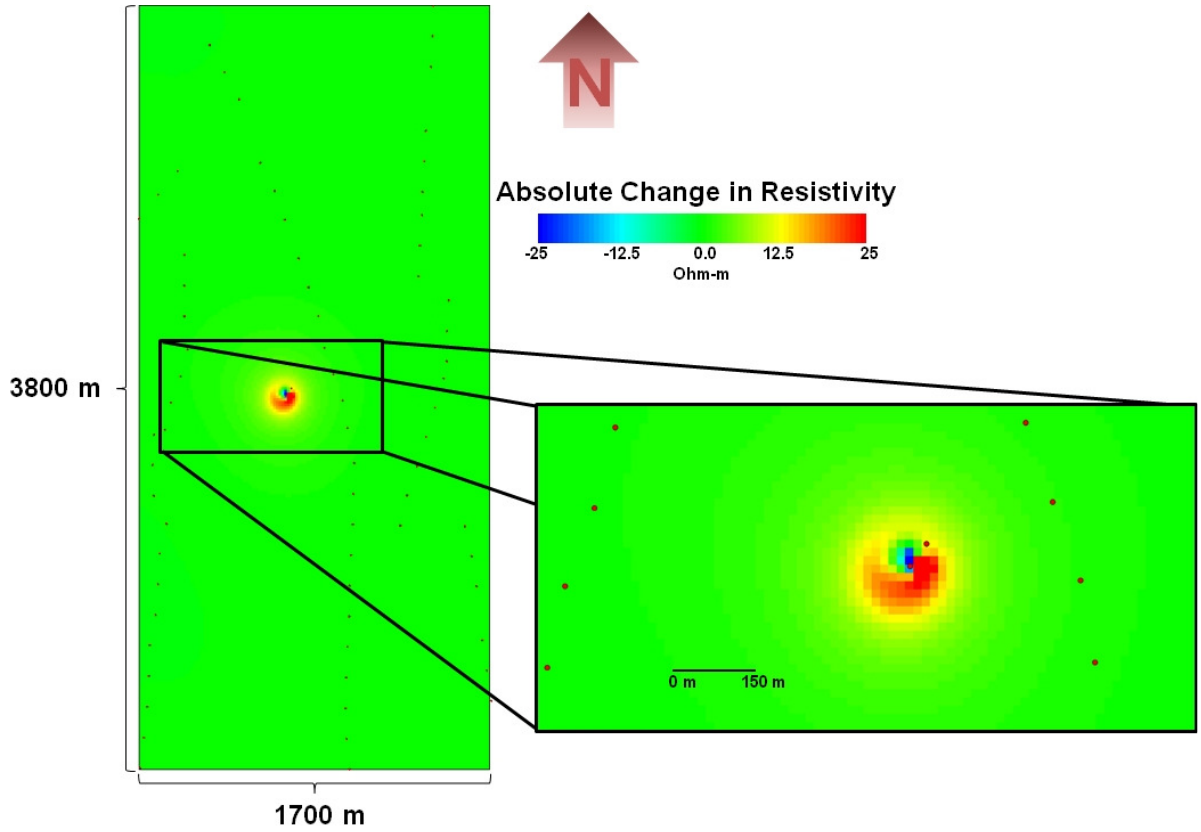

Figure 34. Close up of the absolute change in resistivity around the well at a depth from surface of 635 m.

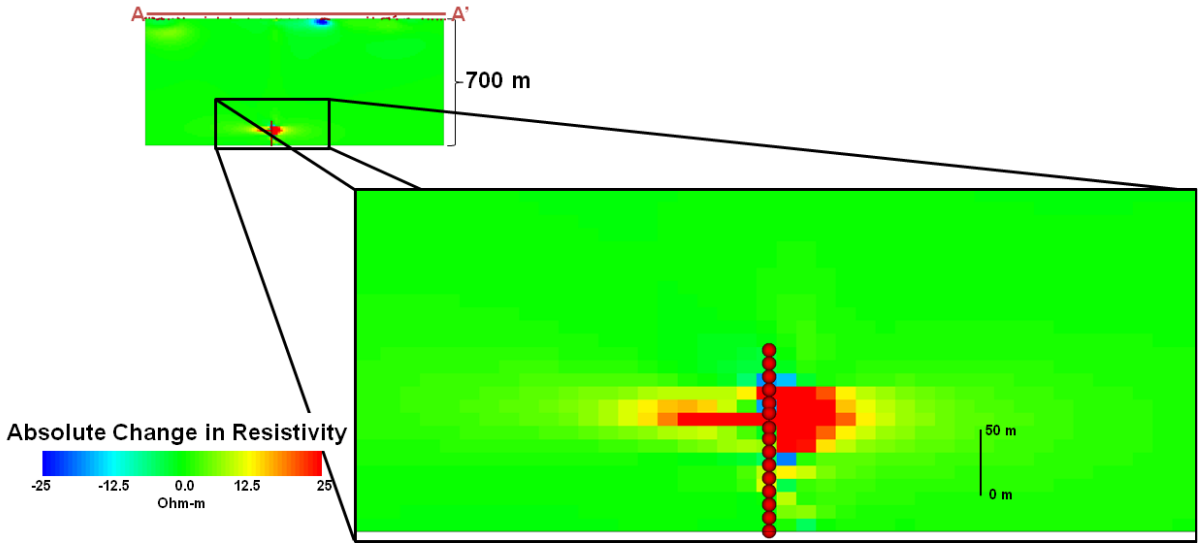

Figure 35. Close up of the absolute change in resistivity around the well from the cross section A-A'.

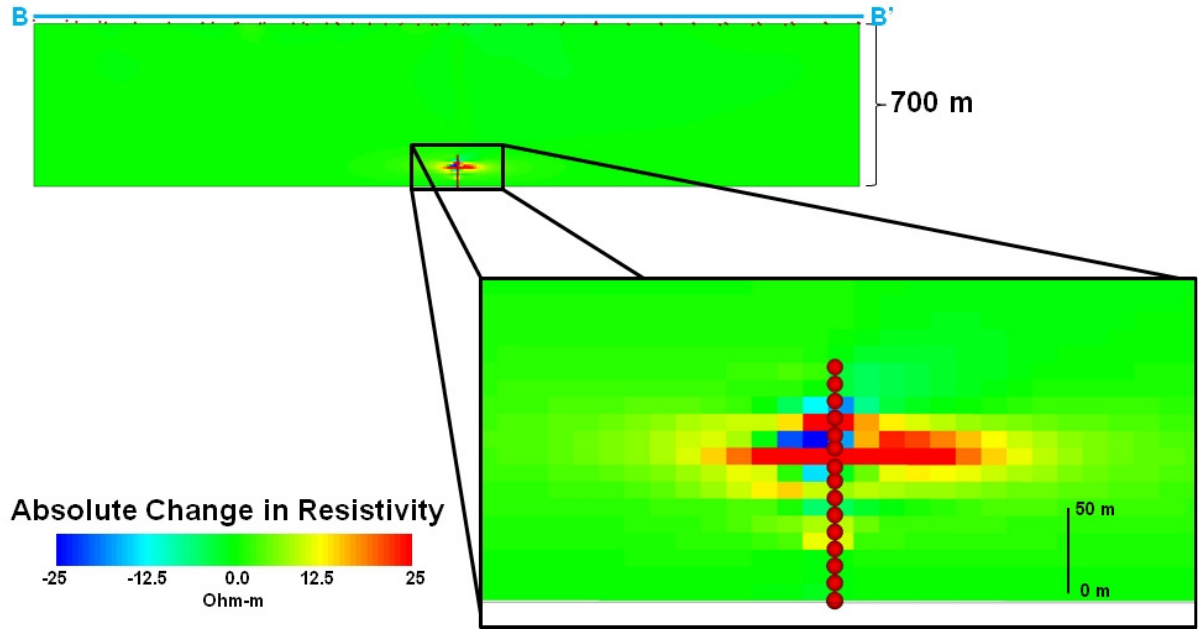

Figure 36. Close up of the absolute change in resistivity around the well from the cross section B-B'.

Comparison with Cross-Hole Results

We compared the CSEM data to cross borehole ERT (XERT) models. Figure 37 shows the XERT surveys between Well 201 (injection well) and Well 200 monitoring well. The pixel size for the XERT images use a fine 3.33 m mesh size. The XERT uses the same logarithmic color scale and range as the preceding resistivity images. Figure 37A represents the cross well image from the September 2015 (Phase II) field campaign. A comparison of the CSEM and XERT images is difficult since the ERT data were inverted using much smaller cells sizes (3.33 x 3.33 x 3.33 m for XERT versus 15 x 15 x 10 m for the CSEM); however, there are similarities between in the CSEM and ERT images. Figure 37B shows the cross well image from the April 2016 (Phase III) field campaign. Again, it is somewhat difficult to compare the XERT and CSEM images as the ERT images are higher resolution and show much more complex changes. Part of these changes may be artifacts of damage to the electrodes and/or well casing coating. At the depths of the injection zone (red bar on the right of Figure 37A) and close to the casing (left side of both images), the resistivity appears to decrease. Overall, the resistivity appears to increase particularly at shallow depths and away from the well casing.

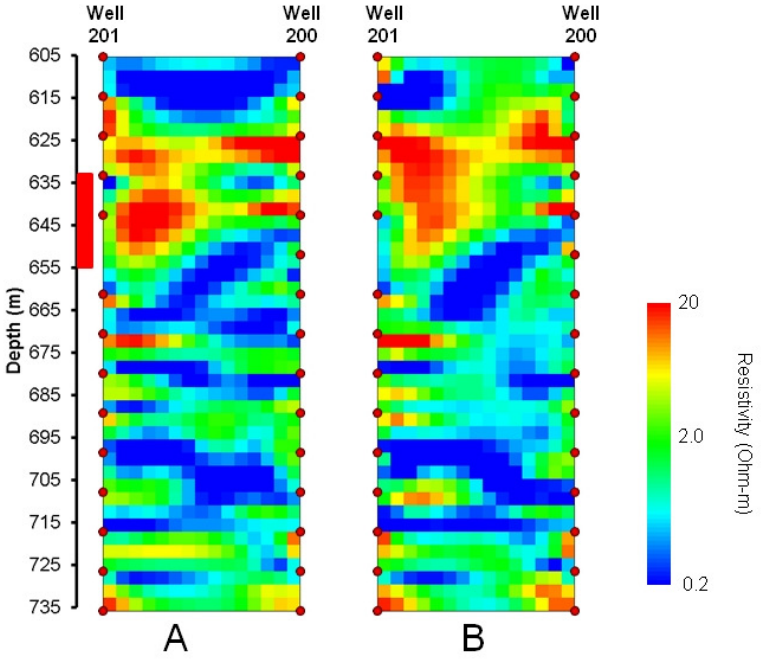

Figure 37. Cross borehole ERT of the A) Phase II (pre-brine injection) field campaign and B) Phase III (post brine injection) field campaign. The red box on the scale represents the location of the screen used for injection in Well 201.

Additional validation of results includes the analysis from LBNL (Petrov, 2016). LBNL used a mesh of 25 m around the injection well and made a continuously increasing grid size up to 200

meters near the boundary of the inversion. The data used for the LBNL finite-difference inversion included frequency ranges between 0.125 and 7.5 Hz. LBNL also constrained the data using electrical conductivity boundaries of $5x10^{-3}$ and 12 S/m. The inversion uses a regularization parameter (λ) of 100 then after 150 iterations, λ is reduced to 0.025. Overall the inversion required 30,000 computer cores of a massively parallel computer from the National Energy Research Scientific Computing Center (NERSC) (Petrov, 2016). Although the LBNL grid size is larger than MPT's grid size, they are comparable.

The LBNL report shows the absolute difference in conductivity from Trip 4 (Phase III) and Trip 3 (Phase II). Figure 38 shows the cross section of the XZ plane (Figure 38A) and the cross section of the YZ plane (Figure 38B). Figure 38A correlates with the XZ cross section of the absolute resistivity as shown in Figure 35. The electrical conductivity difference size is similar. Figure 38B shows the YZ cross section, which is comparable to the B-B' cross section shown in Figure 36 as well. The absolute difference in conductivity in both figures shows a decrease in conductivity. This is comparable to the results shown in MPT's absolute difference increase in resistivity with approximately the same depths.

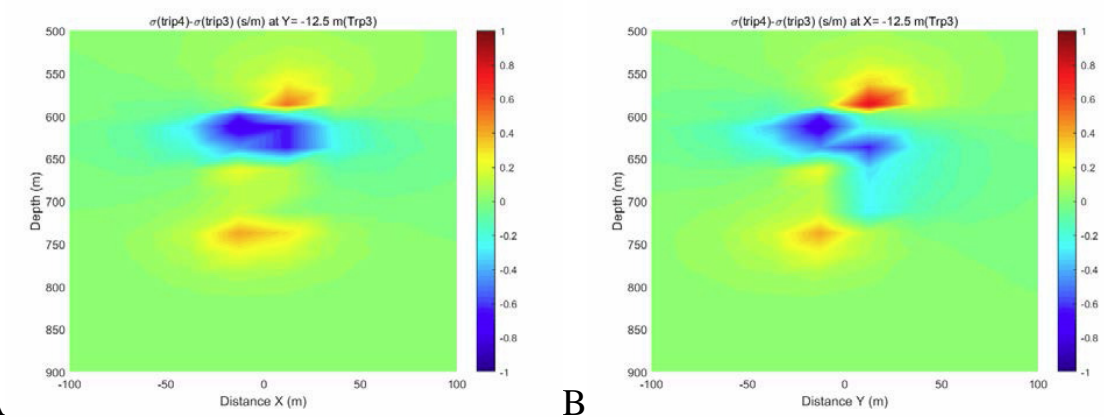

A B

Figure 38. Results of the LBNL finite-difference inversion using electrical conductivity with a view of the A) XZ cross section near Well 201and B) YZ cross section near Well 201.

Conclusions

Lessons learned during the Phase I field deployment resulted in changes in the field approach for the Phase II and Phase III field data acquisition and field set up. The Phase II and Phase III field set up focused on the high density surface array. This array minimized the effect of the gas pipelines near the Ketzin site; however, the gas pipelines still affected the signal-to-noise ratio on the CSEM data. In addition, the high traffic area, nearby electric railway, and wind and solar farms all had an effect on the signal to noise ratio.

Initial data analysis provided an expected image of the site using the high-density multisource array. However, additional and highly thorough analysis of the Phase II and Phase III data determined issues with the data. The issues included three borehole electrodes (borehole electrodes 2, 7 and 9) which appear to be increasingly noisy, damage to the lightning protection system at the wellhead which implies the occurrence of a high current event, such as a lightning strike, that impacted the system and damaged the fiberglass coating on the metal boreholes.

MPT was able to develop solutions to the issues. Which include the elimination of the faulty electrodes from the Phase II and Phase III data, determining that the damaged surge protection may not have significantly impacted the data, and fixing the borehole coating failure issue during the data inversion process by shifting the borehole one cell in the X-direction. The resultant inversion provided the best fit models for Phase II and Phase III.

Overall, there appears to be an increase in resistivity of the CO_2 plume from the Phase II field campaign to the Phase III field campaign. This appears to be counterintuitive to the known field activity that occurred between the Phase II (September 2015) and Phase III (April 2016) campaigns since the GFZ injected a brine solution in January 2016.

The brine solution should have had a resistivity similar to the background resistivity of the reservoir (approximately 3.8 ohm-m). This should have created a decrease in resistivity of the CO_2 plume surrounding the injection well. Therefore, MPT conducted an additional analysis by comparing the absolute resistivity change between Phase II and Phase III and also compared the CSEM data to cross borehole ERT models.

The models and analysis provide the same conclusion that there is an increase in resistivity between the Phase II and Phase III data. However, both the CSEM and cross borehole ERT show intermittent decreases in resistivity along the borehole, which may indicate the injection of the brine solution in the reservoir.

Bibliography

Arts, R., O. Eiken, A. Chadwick, P. Zweigel, L. Van Der Meer, and B. Zinszner, 2004, Monitoring of CO2 injected at Sleipner using time-lapse seismic data: Energy, 29, 1383–1392.

Bergmann, P., Schmidt-Hattenberger, C., Kiessling, D., Rücker, C., Labitzke, T., Henninges, J., Baumann, G., and Schütt, H., 2012, Surface-downhole electrical resistivity tomography applied to monitoring of CO2 storage at Ketzin, Germany, Geophysics, 77, 253–267

Constable, S., 2010, Ten years of marine CSEM for hydrocarbon exploration: Geophysics 75 (5), 75A67-75A81.

Gasperikova, E. and G. Hoversten, 2006, A feasibility study of non-seismic geophysical methods for monitoring geologic CO2 sequestration: Society of Exploration Geophysicists, The Leading Edge, 1282-1288.

GTPro Geotechnologie GmbH, Berlin (Germany). (2012). Gas Pipeline map. Unpublished manuscript.

Ivanova, A., A. Kashubin, N. Juhojuntti, J. Kummerow, J. Henninges, C. Juhlin, S. Lüth, and M. Ivandic, 2012, Monitoring and volumetric estimation of injected CO2 using 4D seismic, petrophysical data, core measurements and well logging: A case study at Ketzin, Germany: Geophysical Prospecting, 60, 957–973.

Kiessling, D., C. Schmidt-Hattenberger, H. Schütt, F. Schilling, K. Krüger, B. Schöbel, E. Danckwardt, J. Kummerow, & CO2SINK Group, 2010, Geoelectrical methods for monitoring geological CO2 storage: First results from crosshole and surface-downhole measurements from the CO2SINK test site at Ketzin (Germany): International Journal of Greenhouse Gas Control 4, 816-826.

Newman, G. A. and Alumbaugh, D. L., 1995, Frequency-domain modelling of airborne electromagnetic responses using staggered finite differences. Geophysical Prospecting, 43, 1021–1042.

Petrov, P. (2016), Controlled-Source Electromagnetic Inversion Applied to Imaging of CO2 Storage at Ketzin, Germany. Unpublished manuscript.

Um, E. S., Daley T., Newman, G., LaBrecque, D., and Brigham, R., (2014). Quick Look Report: Preliminary Model Study for EM Modeling and Design. Unpublished manuscript.

Um, E. S., (2015). Ketzin STB CSEM Inversion. Unpublished manuscript.

White, D. 2009, Monitoring CO2 storage during EOR at the Weyburn–Midale Field: The Leading Edge, 28, 838–842.

Yang, X., C. Carrigan, D. J. LaBrecque, A. Ramirez, R. Aines, S. J. Friedman, and S. Hvorka, 2012, Interpretation of noisy time lapse Electrical Resistivity Tomography data: Society of Exploration Geophysicists.